Science of the Total Environment 838 (2022) 156592

Contents lists available at ScienceDirect

Science of the Total Environment

journal homepage: www.elsevier.com/locate/scitotenv

Evidence for enhanced primary production driving significant CO_2 drawdown associated with the Atlantic ITCZ

J. Severino P. Ibánhez [a,b,*], Manuel Flores Montes [c], Nathalie Lefèvre [d]

[a] Instituto de Investigacións Mariñas, Consejo Superior de Investigaciones Científicas (IIM-CSIC), Eduardo Cabello 6, 36208 Vigo, Spain
[b] Biogeochemistry Research Group, School of Natural Sciences, Trinity College Dublin, College Green, Dublin 2, Ireland
[c] Department of Oceanography – DOCEAN, Federal University of Pernambuco – UFPE, Av. Arquitetura, s/n, Cidade Universitária, 50740-550 Recife, PE, Brazil
[d] IRD-LOCEAN, Sorbonne Université, 4 place Jussieu, 75252 Paris Cedex 05, France

HIGHLIGHTS

- Rainfall associated with the Atlantic ITCZ promotes a large reduction of oceanic CO_2 emissions to the atmosphere.
- Thermodynamics and physics only explain 41% of the observed CO_2 drawdown associated with rainfall in the tropical Atlantic.
- The freshening caused by the ITCZ seems to enhance primary production in the otherwise oligotrophic tropical Atlantic.

GRAPHICAL ABSTRACT

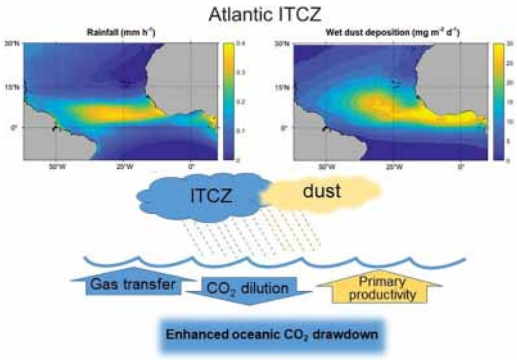

ARTICLE INFO

Editor: Julian Blasco

Keywords:
Tropical Atlantic
Oceanic carbonate system
Sea-air CO_2 flux
Rainfall
Diazotrophy

ABSTRACT

The intense rainfall associated with the Intertropical Convergence Zone (ITCZ), a narrow zone of confluence of the northeast and southeast trades, can significantly alter sea surface salinity, the chemistry of inorganic C and the resulting sea-air CO_2 exchange in the tropics. We have analyzed extensive underway data collected from 2008 until 2014 and recorded by an autonomous CO_2 system installed on a commercial ship that crosses the central tropical Atlantic (5°S to 15°N, 18°W to 36°W) to disentangle the effects of the ITCZ over the carbonate system there. Based on statistically significant linear co-variance of sea surface fugacity of CO_2 (fCO_{2sw}) and sea surface salinity in the areas affected by the ITCZ, we calculated CO_2 drawdown rates associated with the impact of the ITCZ in the central tropical Atlantic ranging from 0.11 ± 0.02 to 2.35 ± 0.08 mmol m^{-2} d^{-1}. These were calculated by comparing the observed fCO_{2sw} with that expected without surface seawater carbonate system dilution and increase in gas transfer caused by the ITCZ. The observed decrease in fCO_{2sw} associated with the freshening caused by the ITCZ is much larger than expected from thermodynamics alone. 59.1 ± 4.1 % of the total observed CO_2 drawdown associated with the ITCZ cannot be explained by abiotic processes. Instead, we found significant negative correlations between underway sea surface salinity and remote-sensed chlorophyll *a* in the areas affected by the ITCZ. Different to other tropical oceanic basins, the tropical Atlantic receives large amounts of continental dust originated from Africa. Wet dust deposition driven by the ITCZ appears associated with the interannual variability of the CO_2 drawdown associated with the ITCZ. Fertilization driven by the ITCZ seems to enhance primary production in the otherwise oligotrophic tropical Atlantic, thus significantly lowering CO_2 emissions to the atmosphere.

* Corresponding author at: Instituto de Investigacións Mariñas, Consejo Superior de Investigaciones Científicas (IIM-CSIC), Eduardo Cabello 6, 36208 Vigo, Spain.
E-mail address: jseverino@iim.csic.es (J.S.P. Ibánhez).

http://dx.doi.org/10.1016/j.scitotenv.2022.156592
Received 11 January 2022; Received in revised form 14 May 2022; Accepted 6 June 2022
Available online 8 June 2022

1. Introduction

The global ocean is a net sink of atmospheric CO_2, absorbing about 23 % of the anthropogenic CO_2 emissions to the atmosphere during the last decade (Friedlingstein et al., 2020). Nevertheless, sea-air CO_2 fluxes are not uniformly distributed throughout the ocean's surface. Since atmospheric CO_2 has a relatively homogeneous global distribution, the role of ocean's surface as a source or a sink of atmospheric CO_2 depends on the distribution of the fugacity of CO_2 (fCO_2) in surface seawaters. Thus, the tropical band is generally a source of CO_2 to the atmosphere due to high sea surface temperatures (SST) and the equatorial upwelling of CO_2-rich waters (e.g. Landschützer et al., 2016; Takahashi et al., 2014). The tropical Atlantic is the second largest oceanic CO_2 source to the atmosphere after the tropical Pacific, largely fuelled by the zonal spread of CO_2-rich waters originated in the equatorial upwelling (Andrié et al., 1986). Nevertheless, different to the tropical Pacific, the tropical Atlantic receives the discharge of some of the largest rivers in the world, such as the Amazon, Niger and Congo rivers, that spread through vast areas beyond the coastal zone driven by the prevailing winds and complex surface currents (Bianchi and Allison, 2009). These large outer river plumes are significant atmospheric CO_2 sinks due to enhanced primary production in the otherwise oligotrophic tropical Atlantic (Cooley et al., 2007; Ibánhez et al., 2015; Körtzinger, 2003, 2010; Lefèvre, 2009; Lefèvre et al., 2017a; Ternon et al., 2000). The zonal spread of these continental freshwater sources further overlaps with the freshening caused by the Intertropical Convergence Zone (ITCZ), significantly affecting the fCO_2 of surface waters across the basin (Ibánhez et al., 2016; Lefèvre et al., 2010; Oudot et al., 1995).

The ITCZ is a narrow zonal band of intense rainfall located in the zone of confluence of the northeast and southeast trades, where they converge to form the rising branch of the Hadley circulation, accounting for 32 % of the global rainfall (Kang et al., 2018). The ITCZ seasonally migrates following the hemispheric asymmetry of SST, being at its northernmost location during boreal summer-early autumn (Donohoe et al., 2013; Kang et al., 2018). The intensity of the rainfall associated with the ITCZ in the tropical ocean is capable of significantly changing sea surface salinity (SSS) and SST across the basin (e.g. Dessier and Donguy, 1994; Grodsky et al., 2020). This freshening caused by the ITCZ dilutes both sea surface total alkalinity (TAlk) and dissolved inorganic C (DIC), enhanced by density stratification, thus lowering sea surface fCO_2 (fCO_{2sw}) and increasing pH (Ashton et al., 2016; Ho and Schanze, 2020; Turk et al., 2010; Woolf et al., 2019). Rainfall is also responsible for the transport of CO_2 to surface waters, termed wet deposition, although a general drop of fCO_{2sw} caused by rainfall prevails (Sarmiento and Gruber, 2006; Turk et al., 2010). Rainfall further enhances sea-air CO_2 exchange rates by increasing gas transfer at the seawater surface through turbulence caused by rain drops (Harrison et al., 2012; Ho et al., 2000). This effect of rain over the gas transfer at the sea surface decreases at increasing wind speeds (Harrison et al., 2012). Combined, the physical and thermodynamic effects of rainfall over the sea-air exchange of CO_2 can either reduce CO_2 emissions in areas of CO_2 outgassing or enhance sea surface CO_2 uptake in oceanic CO_2 sink areas (Ho and Schanze, 2020), thus significantly impacting sea-air CO_2 exchange globally (Ashton et al., 2016).

A lowering of the fCO_{2sw} proportional to SSS changes caused by the rainfall associated with the ITCZ has been observed in the tropical Pacific (Ho and Schanze, 2020; Turk et al., 2010), as well as in the tropical Atlantic (Lefèvre et al., 2010; Oudot et al., 1995). In the tropical Pacific, the physical and thermodynamic effects of rainfall over the carbonate system successfully explained the observed fCO_{2sw} in the areas affected by the ITCZ (Ho and Schanze, 2020; Turk et al., 2010). Different to the tropical Pacific and adding to the spatial overlapping of the freshening caused by the ITCZ and the zonal spread of large river plumes, the tropical Atlantic receives the largest fluxes of continental dust of all oceans originating from northwest Africa (Mahowald et al., 2009) that crosses the basin reaching the Caribbean Sea and America (Prospero et al., 2014). Wet deposition associated with the ITCZ is one of the main transport pathways of these particles (van der Does et al., 2020), thus fertilizing vast oligotrophic oceanic areas (Schlosser et al., 2014). This raises high uncertainties about the expected role of the ITCZ in the sea-air CO_2 exchange in the tropical Atlantic. Nevertheless, the drivers of surface seawater carbonate system variability in the areas affected by the ITCZ in the tropical Atlantic have not been addressed to date.

In this study, we use routine underway measurements performed along a commercial line between France and Brazil that crosses the central tropical Atlantic. The spatial and temporal coverage of the underway measurements performed permit to obtain a complete picture of the seasonal influence of the ITCZ over fCO_{2sw} in the area. The main objective of this study is therefore to evaluate the impact of the intense rainfall associated with the ITCZ over the fCO_{2sw} and sea-air CO_2 fluxes in the tropical Atlantic. The recorded underway fCO_{2sw} is compared to that expected from thermodynamics and the main drivers of the observed changes in the local carbonate system are disentangled.

2. Materials and methods

2.1. Underway measurements and sea-air CO_2 exchange

An automated CO_2 equipment based on infrared detection (LI-COR Inc. model 7000, Lincoln, USA; Pierrot et al., 2009) was installed on board commercial vessels since 2008 sailing the commercial route Le Havre (mainland France) – Santos (Brazil), consecutively on the Motor Vessel (MV) Monte Olivia (2008–2009), MV Rio Blanco (2009–2012), MV Santa Cruz (2013–2014) and MV Cap San Lorenzo (2014 onwards; Table 1). During the ships' voyages, underway fCO_{2sw} and atmospheric fCO_2 (fCO_{2atm}) determinations were made. A thermosalinograph (SeaBird Scientific model SBE-21, Bellevue, USA) and a barometer (Druck model RPT350, Baker Hughes Company, Leicester, UK) were also installed in the vessels, thus measuring underway SST, SSS and atmospheric pressure (Pres). In this study, we use ships' voyages from 2008 until 2014 that recorded sufficient data in the area of influence of the ITCZ in the tropical Atlantic (Fig. 1). Data used were collected between 15°N and 5°S (Lefèvre and Diverrès, 2021a,b) from 35 voyages (Table 1).

During March and April 2011, the atmospheric molar fraction of CO_2 (xCO_{2atm}) could not be recorded onboard the MV Monte Olivia due to a problem with the atmospheric pumping. For this period, the ship atmospheric measurements are replaced by the monthly xCO_{2atm} recorded at the atmospheric stations of the NOAA/ESRL Global Monitoring Division (http://www.esrl.noaa.gov/gmd/ccgg/iadv/) of Ascension Island (7.97°S, 14.40°W), Farol De Mae Luiza Lighthouse (5.80°S, 35.19°W; data since 2010), Ragged Point (13.17°N, 59.43°W) and Tenerife (28.31°N, 16.50°W) are used. Monthly xCO_{2atm} measurements at these stations are linearly interpolated at the position of the underway measurements. fCO_{2atm} is then calculated as

$$fCO_{2atm} = xCO_{2atm}(Pres - pH_2O)\, C \quad (1)$$

where pH_2O is the water vapor pressure at 100 % humidity calculated from underway SST and SSS, and C is the fugacity coefficient calculated from Weiss (1974). The same procedure is used to calculate fCO_{2atm} along the tracks of the voyages where underway XCO_{2atm} was measured. Comparison of both calculated and measured fCO_{2atm} gives very good results, with deviations (average 1.70 μatm, n = 40,925; see Supplementary materials) within the precision range of the equipment (<2 μatm).

Sea-air CO_2 fluxes (F) are calculated according to

$$F = k_{total}\, S_o (fCO_{2sw} - fCO_{2atm}) \quad (2)$$

where S_o is the solubility of CO_2 (Weiss, 1974) and k_{total} is the gas transfer velocity. Both wind speed and rainfall enhance sea-air gas exchange by affecting k_{total} in a nonlinear manner (Harrison et al., 2012):

$$k_{total} = k_{wind} + [1 - \exp(-\alpha\beta)]k_{rainfall} \quad (3)$$

where k_{wind} is the gas transfer velocity associated with the wind solely, $k_{rainfall}$ is that promoted by rainfall solely, α is a non-dimensional fitting

Table 1
VOS voyages used in this study. The limits of the ship tracks used here and the dates the ship performed each track are also shown.

ID	Dates of the voyages	Name	Minimum latitude	Maximum latitude	Representative month
1	15–18 July 2008	MV Monte Olivia	5°S	15°N	July
2	8–10 October 2008	MV Monte Olivia	5°S	15°N	October
3	19–21 November 2008	MV Monte Olivia	4°S	15°N	November
4	9–11 December 2008	MV Monte Olivia	5°S	15°N	December
5	1–3 January 2009	MV Monte Olivia	5°S	14°N	January
6	20–23 January 2009	MV Monte Olivia	5°S	15°N	January
7	11–13 February 2009	MV Monte Olivia	5°S	15°N	February
8	3–6 March 2009	MV Monte Olivia	5°S	15°N	March
9	14–17 April 2009	MV Monte Olivia	5°S	15°N	April
10	15–18 December 2009	MV Rio Blanco	5°S	15°N	December
11	20–23 January 2010	MV Rio Blanco	5°S	15°N	January
12	10–12 February 2010	MV Rio Blanco	5°S	15°N	February
13	3–6 March 2010	MV Rio Blanco	5°S	15°N	March
14	23–26 March 2010	MV Rio Blanco	5°S	15°N	March
15	9–12 May 2010	MV Rio Blanco	5°S	15°N	May
16	4–7 June 2010	MV Rio Blanco	5°S	15°N	June
17	28 June-1 July 2010	MV Rio Blanco	5°S	15°N	June
18	22–26 July 2010	MV Rio Blanco	5°S	15°N	July
19	15–18 August 2010	MV Rio Blanco	5°S	15°N	August
20	9–13 September 2010	MV Rio Blanco	5°S	15°N	September
21	28–30 October 2010	MV Rio Blanco	5°S	15°N	October
22	24–28 March 2011	MV Rio Blanco	5°S	15°N	March
23	18–20 April 2011	MV Rio Blanco	5°S	15°N	April
24	12–16 May 2011	MV Rio Blanco	5°S	15°N	May
25	4–7 June 2011	MV Rio Blanco	5°S	15°N	June
26	30 June–4 July 2011	MV Rio Blanco	5°S	15°N	July
27	23–26 July 2011	MV Rio Blanco	5°S	15°N	July
28	6–9 June 2012	MV Santa Cruz	5°S	15°N	June
29	1–4 July 2012	MV Santa Cruz	5°S	15°N	July
30	20–22 August 2012	MV Santa Cruz	5°S	15°N	August
31	13–15 September 2012	MV Santa Cruz	5°S	10°N	September
32	4–7 April 2013	MV Santa Cruz	5°S	15°N	April
33	28 April–1 May 2013	MV Santa Cruz	5°S	15°N	April
34	23–26 January 2014	MV Santa Cruz	5°S	15°N	January
35	11–15 December 2014	MV Cap San Lorenzo	5°S	15°N	December

parameter of the empirical Eq. (3) and β is the ratio between the kinetic energy flux caused by rainfall (KEF_{rain}) and that caused by wind (KEF_{wind}). KEF_{rain} can be simplified to $KEF_{rain} = 0.0112\ Rn$ (Harrison et al., 2012), where Rn is the rainfall rate, while KEF_{wind} can be calculated as:

$$KEF_{wind} = \rho C_d U_{10}^2 \quad (4)$$

where ρ is the air density and C_d is the drag coefficient. $k_{rainfall}$ and k_{wind} are calculated following the parametrizations made by Harrison et al. (2012) and Ho et al. (2006), respectively:

$$k(600)_{rainfall} = 63.02(KEF_{rain})^{0.6242} \quad (5)$$

$$k(600)_{wind} = 0.266\ U_{10}^2 \quad (6)$$

where U_{10} is the wind speed at 10 m height above sea surface.

2.2. Remote-sensed and reanalysis data

U_{10} is obtained from the European Centre for Medium-Range Weather Forecasts (ECMWF) daily reanalysis data (ERA-interim, 0.125° resolution). Daily rainfall data are obtained from the Tropical Rainfall Measuring Mission (TRMM) (Huffman et al., 2007) (http://precip.gsfc.nasa.gov/; 0.25° resolution). In both cases, the regular grid of daily data was linearly interpolated at the position of each underway measurement and using the date of passage (Table 1).

U_{10} is used to calculate wind stress (τ) and thus, Ekman pumping (We) from the equation (Pickett and Paduan, 2003):

$$W_e = Curl\left(\frac{\tau}{\rho f}\right) \quad (7)$$

where ρ is the density of seawater (assumed 1025 Kg m^{-3}) and f is the Coriolis parameter.

Rainfall events can promote stratification in the open ocean that can last for several hours depending on factors such as wind speed or surface current velocity (Boutin et al., 2015). The gridded daily rainfall TRMM data are additionally used to identify the areas affected by recent rainfall along the tracks of the VOS used here. The accumulated rainfall corresponding to a four days period prior the passage of the ships was linearly interpolated at the position of the underway measurements. This arbitrary integration time-period was varied (±2 days) offering highly similar results (data not shown). An accumulated rainfall threshold of 1 mm is used to discern among areas affected and not affected by recent rainfall.

Sea surface current velocities obtained from the Ocean Surface Current Analyses – Real time (OSCAR) data (1/3° resolution; JPL Physical Oceanography DAAC; developed by ESR) are used to separate the different surface waters and thus avoid fCO_{2sw} changes caused by the mixture of oceanic water masses with different origin and carbonate system properties. In this case, we opt for using the monthly OSCAR product to avoid surface water masses misidentification due to short-term reversal of surface water direction. Sea surface circulation in the tropical Atlantic is dominated by the zonal component, with the westward North Equatorial Current (NEC) and South Equatorial Current (SEC) separated by the eastward North Equatorial Countercurrent (NECC; Fig. 1). The SEC further presents three branches, although only two appear in the study area (Fig. 1), separated by the South Equatorial Undercurrent (Stramma, 1991). At the surface, the divide between the two branches of the SEC in the study area varies seasonally from westward to eastward propagation (Stramma, 1991). The gridded zonal component of the OSCAR dataset was linearly interpolated at the position of each underway measurement and used to identify the limits of the three main surface currents in the study area. From North to South, the limit of the NEC is stablished where the zonal component of the velocity changes to eastward propagation when the NECC is present,

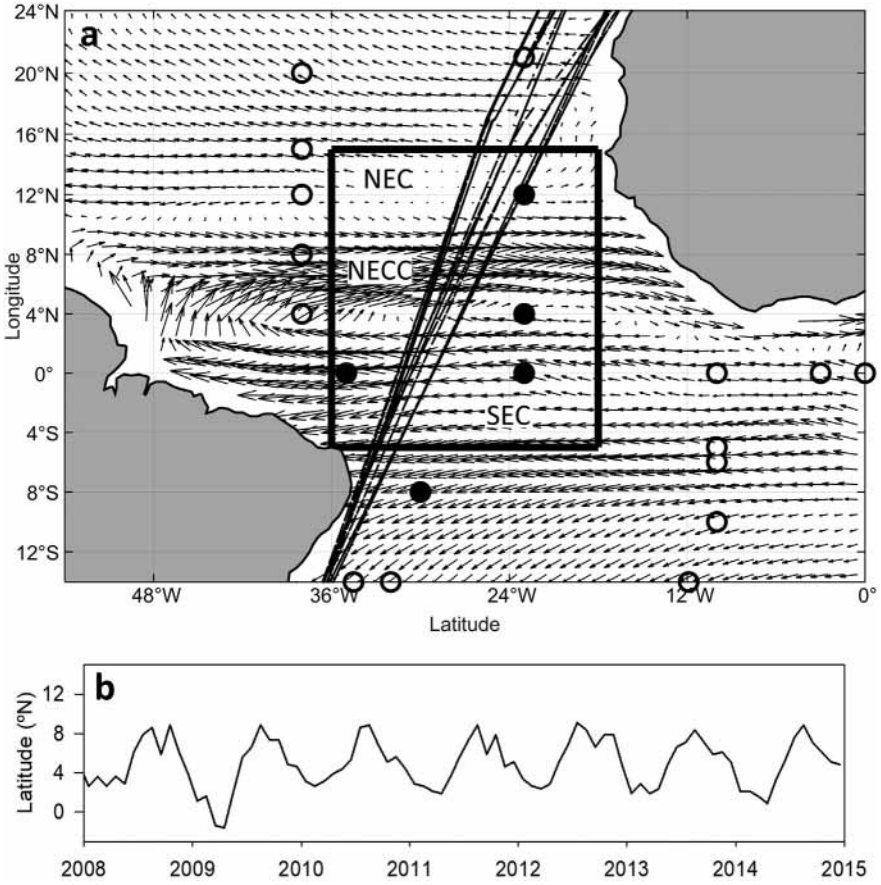

Fig. 1. a. Tracks of the 35 ships' voyages of the voluntary observing ships (VOSs) crossing the tropical Atlantic and used in this study. The long-term mean surface velocity for the month of August (calculated for the 1998–2014 period) is shown, with the indication of the main surface currents present in the studied area (marked square): the North Equatorial Current (NEC), the North Equatorial Countercurrent (NECC) and the South Equatorial Current (SEC). The location of the Prediction and Research Moored Array in the Tropical Atlantic (PIRATA; Bourlès et al., 2019) is also shown (circles), together with the moorings used in this study (black circles). b. Monthly latitudinal ITCZ position calculated as the monthly maximum precipitation latitudinal band within 5°S–15°N and averaged for the 18–36°W longitudinal band.

or until an intensification of the westward propagation caused by the SEC when the NECC is not present. The NECC is identified as the area with eastward surface water propagation in the 3–10°N latitudinal band, between the SEC and the NEC. Finally, the two branches observed in the SEC are assumed to have similar carbonate system characteristics and included in a single SEC discrimination.

The reliability of remote-sensed wind speed, rainfall and the zonal component of surface currents obtained from reanalysis was tested by comparing them with those properties measured in the Prediction and Research Moored Array in the Tropical Atlantic (PIRATA; Bourlès et al., 2019; Fig. 1). Remote-sensed and reanalysis properties were linearly interpolated at the location of the five (two with available surface current data) PIRATA moorings closer to the study area framed in Fig. 1 (5°S to 15°N, 18°W to 36°W). Both sets of data showed very good agreement for the 2008–2014 period (see Supplementary materials).

Additionally, remote-sensed, monthly-averaged Chlorophyll *a* (Chl *a*) concentration, reanalysis wet and dry dust deposition rates and remote-sensed SSS are used in this study. Monthly-averaged Chl *a* concentration is obtained from the Moderate Resolution Imaging Spectroradiometer (MODIS)/Aqua satellite with a 4 km resolution and processed with the OC3M algorithm and standard NASA global coefficients (O'Reilly et al., 1998). The monthly data are linearly interpolated at the position of each underway measurement. Monthly wet and dry dust deposition rates are obtained from the NASA's Modern-Era Retrospective Analysis for Research and Applications, version 2 (MERRA-2), produced by the Goddard Earth Observing System-Data Assimilation System (GEOS-DAS, version 5.12.4; Gelaro et al., 2017). MERRA-2 provides monthly dust deposition reanalysis data from 1980 with a spatial resolution of 0.5° latitude and 0.66° longitude and discriminated into 5 dust size bins. The total wet and dry dust deposition rates are calculated by summing up the 5 dust size classes. Finally, monthly SSS data (0.25° resolution) are obtained from the Soil Moisture and Ocean Salinity (SMOS) mission, available from the Ocean Salinity Expertise Center (CECOS), IFREMER (France).

Rainfall and wet and dry dust deposition climatologies in the area of study are computed as the long-term (1998–2014), monthly average in the area framed within 5°S-15°N and 18°W-36°W (Fig. 1). The period used to calculate these climatologies is arbitrarily chosen to obtain a long-term mean of these properties beyond the period of study, thus limiting the impact of anomalous years over the long-term mean when using short periods. Wet and dry dust deposition and rainfall anomalies are then computed for the studied period (2008–2014). Furthermore, the position of the ITCZ and the maximum wet dust deposition are calculated as the monthly maximum precipitation/wet dust deposition latitudinal band within the same framed area and averaged for the 18°W-36°W longitudinal band.

2.3. Thermodynamic calculations

CO_2 solubility, vapor pressure, fCO_{2sw} and the equilibrium constants of the carbonate system are all affected by SST and SSS changes (Dickson et al., 2007). The overall effect of SST changes over fCO_{2sw} is determined through the thermodynamic coefficient presented by Takahashi et al. (2009):

$$\frac{\partial \ln fCO_{2sw}}{\partial SST} = 0.0433 - 8.7 \times 10^{-5} SST \quad (8)$$

Similarly, Sarmiento and Gruber (2006) describe the effect of SSS variations over fCO_{2sw} when resulting from the admixture of waters with highly different DIC and TAlk content, such as the influence of rainfall on seawater, as:

$$\frac{\partial\ ln\ fCO_{2sw}}{\partial\ ln\ SSS} = \gamma_s + \gamma_{DIC} + \gamma_{TAlk} = \gamma_{rain} \quad (9)$$

where γ_s refers to the effect of SSS changes over the dissociation constants of the carbonate system and is close to 1, and γ_{DIC} and γ_{TAlk} are the sensitivities of fCO_{2sw} to changes in DIC (i.e. Revelle factor) and Talk, respectively. Reported globally averaged values of γ_{rain} range from 1.6 at low latitudes to 1.7 at high latitudes (Sarmiento and Gruber, 2006).

To evaluate the magnitude of each of the thermodynamic terms of Eq. (9) in the tropical Atlantic, we first use the highly significant linear relationship of TAlk with SSS found by Lefèvre et al. (2010) to estimate TAlk

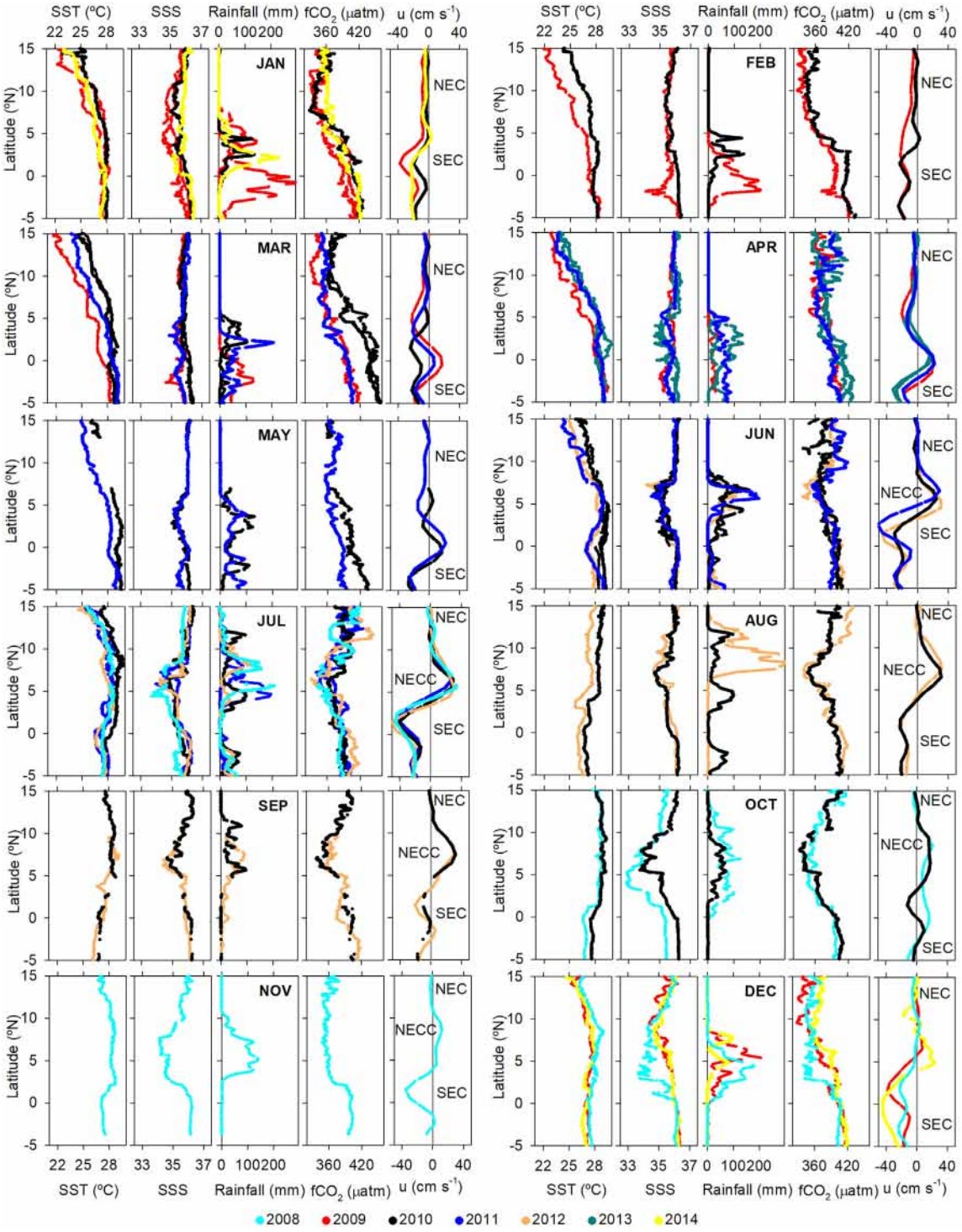

Fig. 2. Latitudinal distribution of sea surface temperature (SST), sea surface salinity (SSS), interpolated rainfall accumulated during the 4 days prior the passage of the VOS, sea surface fCO_2 and the interpolated zonal component of the monthly-averaged surface velocity (u; positive values indicate eastward movement) for the 35 voyages used in this study. Voyages are organized by representative month and year is denoted by the color code. Note that during January 2009, March and June 2010, July 2011 and April 2013 two voyages were performed.

along the tracks. DIC is then estimated from the calculated TAlk, underway fCO_{2sw}, SST and SSS using the CO2SYS program (van Heuven et al., 2011) and the dissociation constants of carbonic acid in seawater found by Mehrbach et al. (1973) refit by Dickson and Millero (1987). Calculated TAlk and DIC are then used to estimate γ_{DIC} and γ_{TAlk} in the areas affected by rainfall associated with the ITCZ as follows:

$$\gamma_{DIC} = (\Delta fCO_2/fCO_2)/(\Delta DIC/DIC) \quad (10)$$

$$\gamma_{TAlk} = (\Delta fCO_2/fCO_2)/(\Delta TAlk/TAlk) \quad (11)$$

To calculate $\gamma_{DIC,}$ we impose a DIC change of 1 μmol Kg^{-1} keeping unvaried TAlk and calculate the resulting fCO_2 using the CO2SYS program. γ_{TAlk} is calculated similarly by imposing a change of 1 μmol Kg^{-1} in TAlk.

To evaluate the effect of the freshening caused by the ITCZ over underway fCO_{2sw} in the tropical Atlantic, we look for significant linear relationships of ln fCO_{2sw} vs ln SSS (Eq. (9)) in the areas directly affected by recent rainfall, i.e. those where the accumulated rainfall in the four days prior the passage of the VOS was higher than 1 mm. The average SST from all the underway determinations used here is first used in Eq. (8) as reference temperature to remove the thermodynamic effect of temperature over fCO_{2sw}.

To evaluate the total contribution of the ITCZ to the sea-air CO_2 exchange in the region, sea-air CO_2 exchange in the regions where significant linear relationships of ln SSS vs ln fCO_{2sw} are found is decomposed as follows:

$$FCO_{2sea-air} = FCO_{2oceanic} + FCO_{2itcz} \quad (12)$$

where $FCO_{2sea-air}$ is the sea-air CO_2 exchange calculated with underway fCO_{2sw} measurements, $FCO_{2oceanic}$ is that expected without the effects of the ITCZ and FCO_{2itcz} is that associated with the overall impact of the rainfall associated with the ITCZ. To estimate $FCO_{2oceanic}$, we first need to estimate an fCO_{2sw} representative of the different surface oceanic waters transported by the surface current system. The broader spatial extent of the freshening caused by the ITCZ often causes a drop in SSS in an entire surface current, particularly in the NECC, and adds to mixing of waters with different origin towards the limits of the different surface currents, thus hindering the association of an fCO_{2sw} value to each of the surface water masses. As a conservative estimate, for each of the areas where significant linear relationships of ln fCO_{2sw} vs ln SSS are found, the highest measured SSS within these relationships is assumed as representative of each of the currents analyzed without the influence of the ITCZ. This is used together with the ln SSS vs ln fCO_{2sw} linear relationships found to calculate an fCO_{2sw} representative of the oceanic waters of each current and thus, to compute $FCO_{2oceanic}$. FCO_{2itcz} is then calculated from the difference between $FCO_{2sea-air}$ and $FCO_{2oceanic}$. Further to this analysis, FCO_{2itcz} is decomposed into:

$$FCO_{2itcz} = FCO_{2thermodynamics} + FCO_{2unknown} \quad (13)$$

where $FCO_{2thermodynamics}$ accounts for the expected impact of the ITCZ over the carbonate system in the area and the enhanced sea-air transfer coefficient caused by rainfall and $FCO_{2unknown}$ denotes the unexplained sea-air CO_2 exchange. We use underway SSS changes and the theoretical γ_{rain} (1.6; Sarmiento and Gruber, 2006) to calculate fCO_{2sw} and thus $FCO_{2thermodynamics}$.

3. Results

3.1. Underway SST, SSS and fCO_{2sw} variability in the central tropical Atlantic

The monthly distribution of the 35 voyages analyzed here show the seasonal variability of the measured properties in the study area (Table 1; Fig. 2). The latitudinal distribution of underway SST in the tropical Atlantic shows a seasonal pattern in the north of the studied region (15°N), with lower temperatures during boreal winter (down to 22 °C; Fig. 2 January to April) and higher during boreal summer (up to 30 °C; Fig. 2 July to October). In the equatorial area, SST shows lower temporal variability, remaining all year-round in between 26 and 30 °C. SSS measured underway shows

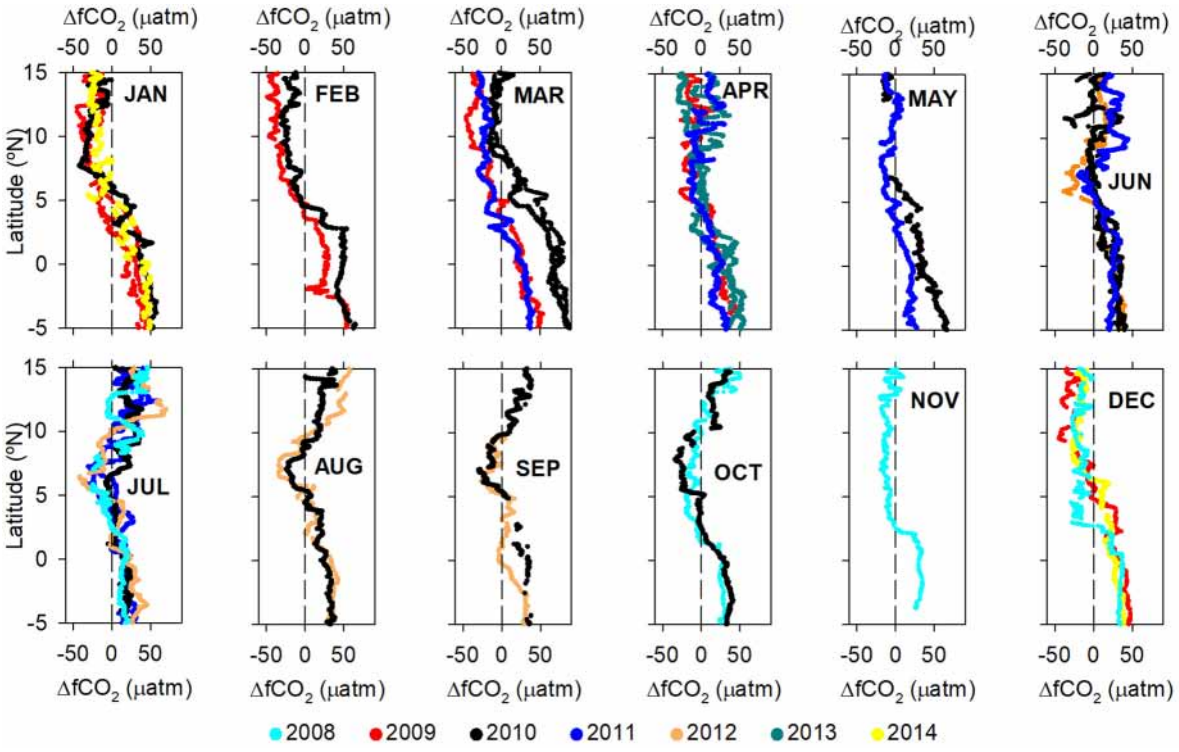

Fig. 3. Latitudinal distribution of ΔfCO_2 calculated for the 35 ships' voyages used here. Year is denoted by the color code. Note that during January 2009, March and June 2010, July 2011 and April 2013 two voyages were performed.

two distinctive areas: one characterized by constant SSS characteristic of oceanic waters, and another one affected by the freshening caused by the intense rainfall associated with the ITCZ and potentially by the Amazon river plume during boreal summer in the NECC (Lefèvre et al., 2020). The position of the ITCZ migrates seasonally and is placed at its northern-most latitude during August/September, and at the southern-most latitude during March to May (Fig. 1; e.g. Lefèvre et al., 2010). This seasonal migration of the position of the ITCZ is observable in the short-term (4 days) rainfall interpolated at the positions of underway measurements used here, with rainfall concentrated in the 5°S-5°N latitudinal band from March to May and in the 5–13°N latitudinal band during August–September (Fig. 2). The location of measured underway SSS minima almost perfectly matches the areas affected by short-term rainfall, thus following the seasonal displacement of the ITCZ (Fig. 2).

Underway fCO_{2sw} shows significant latitudinal gradients associated with the freshening caused by the ITCZ (Lefèvre et al., 2010) and the main system of surface currents in the area (Fig. 2; Lefèvre et al., 2014). As rainfall typically contains no total alkalinity (TAlk) and small amounts of Dissolved Inorganic C (DIC), intense rainfall dilutes these parameters in the surface ocean and promotes a lowering of fCO_{2sw}. This effect can be seen underway in the zones with lower SSS (Fig. 2), and acts together with SST, the surface circulation and the surface transport of different water masses in shaping surface fCO_{2sw} levels.

The three zonal sea surface currents that dominate the circulation in the study area (i.e. the westward NEC and SEC separated by the eastward NECC; Fig. 1) are clearly identified in the interpolated zonal component of the surface circulation obtained from the OSCAR data (Fig. 2). In the southern limit of the studied area, the two branches of the SEC (~5°S-5°N) are identified as two different westward (negative u) maximum zonal velocities, sometimes separated by eastward transport as during March to May (Fig. 2). The SEC transports CO_2-rich waters originated from the equatorial upwelling system and the Benguela Current (e.g. Andrié et al., 1986; Stramma, 1991), which explains the high underway fCO_{2sw} characteristic of the ~5°S-5°N latitudinal band throughout the year outside the areas affected by the ITCZ (Fig. 2). In the northern limit of the studied area, the NEC, mainly fed by the Canary Current that transports waters originated in the Northern hemisphere (e.g. Hernández-Guerra et al., 2005), is characterized by weak westward velocities along the tracks of the vessels used here (Fig. 2; ~5–15°N). There, fCO_{2sw} shows a clear seasonal pattern; lower fCO_{2sw} occurs during boreal winter while the higher fCO_{2sw} in the NEC is verified from June to October. SST is the primary driver of the fCO_{2sw} variability in the NEC (Ibánhez et al.,

Table 2
Impact of the ITCZ over the carbonate system in the tropical Atlantic. ID corresponds to the identification of each VOS voyage used in this study as in Table 1. Data with short-term interpolated rainfall higher than 1 mm was used to obtain the thermodynamic effect of salinity changes caused by rainfall (γ_{rain}) over fCO_{2sw} through linear regression (r) of ln $fCO_{2swnorm}$ vs ln SSS. Estimated fCO_{2sw} sensitivities to DIC (Revelle factor) and TAlk (TAlk sensitivity) changes were used to calculate the expected thermodynamic effect of rainfall over $fCO_{2swnorm}$ (Calc. γ_{rain}) for each voyage used.

ID	Month	Year	Current	SSS range	γ_{rain}	r	Revelle factor	TAlk sensitivity	Calc. γ_{rain}	n
1	7	2008	SEC	34.7–35.7	4.61 ± 0.06	0.95	8.93 ± 0.00	−8.34 ± 0.00	1.59 ± 0.01	558
			NECC	33.7–35.8	2.85 ± 0.08	0.88	8.81 ± 0.00	−8.22 ± 0.00	1.59 ± 0.01	412
2	10	2008	SEC	35.1–35.5	4.98 ± 0.05	0.98	9.06 ± 0.00	−8.46 ± 0.00	1.59 ± 0.00	289
3	11	2008	SEC	34.5–36.2	3.50 ± 0.03	0.98	8.88 ± 0.00	−8.29 ± 0.00	1.59 ± 0.00	360
4	12	2008	SEC	33.7–36.2	2.89 ± 0.04	0.96	8.98 ± 0.00	−8.39 ± 0.01	1.59 ± 0.01	427
5	1	2009	SEC	34.5–36.2	3.45 ± 0.03	0.99	8.93 ± 0.00	−8.34 ± 0.00	1.59 ± 0.01	353
6	1	2009	SEC	35.0–36.1	4.26 ± 0.09	0.88	9.07 ± 0.00	−8.47 ± 0.00	1.60 ± 0.01	687
7	2	2009	SEC	34.1–36.2	1.45 ± 0.02	0.95	9.08 ± 0.00	−8.48 ± 0.00	1.60 ± 0.00	494
8	3	2009	SEC	34.6–36.0	1.97 ± 0.04	0.93	9.06 ± 0.00	−8.46 ± 0.00	1.60 ± 0.00	427
9	4	2009	SEC	35.0–36.0	1.25 ± 0.04	0.84	8.93 ± 0.00	−8.34 ± 0.00	1.59 ± 0.00	368
10	12	2009	SEC	35.6–36.4	4.52 ± 0.12	0.85	9.09 ± 0.00	−8.50 ± 0.00	1.60 ± 0.01	572
			NEC	34.8–35.8	2.66 ± 0.05	0.95	8.83 ± 0.00	−8.25 ± 0.00	1.59 ± 0.00	283
11	1	2010	SEC	35.2–36.3	3.47 ± 0.05	0.95	9.04 ± 0.00	−8.45 ± 0.00	1.60 ± 0.01	440
12	2	2010	SEC	35.4–36.2	3.75 ± 0.04	0.98	9.10 ± 0.00	−8.46 ± 0.00	1.60 ± 0.01	318
15	5	2010	SEC	35.0–36.2	2.92 ± 0.06	0.89	8.90 ± 0.00	−8.31 ± 0.00	1.59 ± 0.00	712
16	6	2010	SEC	35.1–36.2	2.71 ± 0.04	0.92	8.83 ± 0.00	−8.24 ± 0.00	1.59 ± 0.00	806
17	6	2010	SEC	34.8–36.1	3.29 ± 0.03	0.97	8.87 ± 0.00	−8.28 ± 0.00	1.59 ± 0.01	619
			NECC	34.6–35.8	2.15 ± 0.05	0.90	8.77 ± 0.00	−8.19 ± 0.00	1.59 ± 0.00	360
18	7	2010	SEC	35.2–36.1	3.19 ± 0.09	0.84	8.89 ± 0.00	−8.30 ± 0.00	1.59 ± 0.01	594
			NECC	34.8–36.1	2.60 ± 0.04	0.94	8.73 ± 0.00	−8.14 ± 0.00	1.59 ± 0.00	697
19	8	2010	NECC	34.7–36.2	2.77 ± 0.05	0.90	8.77 ± 0.00	−8.19 ± 0.00	1.59 ± 0.00	670
20	9	2010	NECC	34.6–36.3	3.02 ± 0.05	0.92	8.70 ± 0.00	−8.12 ± 0.00	1.58 ± 0.00	636
21	10	2010	SEC	34.1–36.2	4.24 ± 0.07	0.96	8.77 ± 0.00	−8.19 ± 0.00	1.59 ± 0.00	305
			NECC	33.7–36.2	2.56 ± 0.04	0.94	8.67 ± 0.00	−8.09 ± 0.00	1.58 ± 0.01	500
22	3	2011	SEC	34.9–35.9	2.29 ± 0.06	0.79	8.89 ± 0.00	−8.30 ± 0.00	1.59 ± 0.00	830
23	4	2011	SEC	35.3–36.0	2.30 ± 0.07	0.85	8.88 ± 0.00	−8.29 ± 0.00	1.59 ± 0.00	464
24	5	2011	SEC	35.1–36.2	2.89 ± 0.03	0.96	8.81 ± 0.00	−8.22 ± 0.00	1.59 ± 0.00	837
25	6	2011	SEC	35.2–36.3	2.86 ± 0.07	0.88	8.88 ± 0.00	−8.29 ± 0.00	1.59 ± 0.01	445
			NECC	34.5–35.6	2.25 ± 0.06	0.92	8.75 ± 0.00	−8.16 ± 0.00	1.58 ± 0.00	242
26	7	2011	NECC	34.4–36.1	2.45 ± 0.07	0.84	8.75 ± 0.00	−8.16 ± 0.00	1.58 ± 0.01	473
27	7	2011	SEC	35.2–36.3	2.54 ± 0.07	0.91	8.96 ± 0.00	−8.37 ± 0.00	1.59 ± 0.01	303
			NECC	34.0–36.1	3.33 ± 0.07	0.91	8.77 ± 0.00	−8.18 ± 0.00	1.58 ± 0.00	481
28	6	2012	SEC	35.1–36.2	3.52 ± 0.03	0.98	8.97 ± 0.00	−8.38 ± 0.00	1.59 ± 0.01	482
			NECC	34.2–35.5	4.55 ± 0.09	0.96	8.75 ± 0.00	−8.17 ± 0.00	1.58 ± 0.01	217
29	7	2012	SEC	35.4–36.3	4.68 ± 0.06	0.96	9.00 ± 0.00	−8.41 ± 0.00	1.59 ± 0.00	383
			NECC	34.2–35.9	2.53 ± 0.04	0.96	8.76 ± 0.00	−8.18 ± 0.00	1.58 ± 0.01	372
30	8	2012	NECC	34.6–35.9	4.41 ± 0.13	0.89	8.86 ± 0.00	−8.27 ± 0.00	1.59 ± 0.01	293
31	9	2012	NECC	34.4–35.9	2.89 ± 0.07	0.91	8.80 ± 0.00	−8.21 ± 0.00	1.59 ± 0.01	386
32	4	2013	SEC	34.7–36.2	2.35 ± 0.03	0.96	8.99 ± 0.00	−8.39 ± 0.00	1.59 ± 0.00	515
33	4	2013	SEC	35.0–36.2	3.00 ± 0.02	0.98	8.92 ± 0.00	−8.33 ± 0.00	1.60 ± 0.00	585
34	1	2014	SEC	35.2–36.5	2.03 ± 0.03	0.94	9.10 ± 0.00	−8.50 ± 0.00	1.59 ± 0.00	498
			NEC	35.5–36.0	4.38 ± 0.11	0.92	8.93 ± 0.00	−8.34 ± 0.00	1.59 ± 0.00	285
35	12	2014	SEC	35.8–36.4	3.89 ± 0.09	0.91	9.19 ± 0.00	−8.59 ± 0.00	1.60 ± 0.01	389
			NEC	34.7–35.9	3.12 ± 0.02	0.99	8.90 ± 0.00	−8.31 ± 0.00	1.59 ± 0.00	401

2017; Lefèvre et al., 2019) and strongly determines the seasonality observed. In between the SEC and the NEC and from June to November, the northward shift of the trade winds promotes the intensification of the NECC (Fonseca et al., 2004), which becomes visible in the eastward component of the surface velocity centered at about 5°-8°N along the tracks of the vessels used here (Fig. 2, JUN-NOV). Both the CO_2-oversaturated North Brazil Current (Lefèvre et al., 2017b), fed by the SEC, and the NEC can contribute to the water (and carbonate system properties) transported eastward by the NECC (Zhang et al., 2003). Due to the different origin of the waters transported by the surface current system in the study area, the NEC, NECC and SEC present different carbonate system properties reflected in significantly different fCO_{2sw} levels (see Supplementary materials).

The high fCO_{2sw} observed in the 5°S-5°N latitudinal band characteristic of the SEC determines that the waters transported by this current are a permanent source of CO_2 to the atmosphere (i.e. positive ΔfCO_2, Fig. 3). The only exceptions are the areas affected by recent rainfall (Fig. 2), that lowers fCO_{2sw} becoming sporadically a sink of atmospheric CO_2 (e.g. Fig. 3 JUL). Further North, ΔfCO_2 in the NECC shows sea surface CO_2 undersaturation (Fig. 3, JUN-NOV). This is accompanied by a drop in SSS in the latitudinal band of the NECC (Fig. 2, JUN-NOV). During boreal summer, the ITCZ is at its northernmost location and the associated rainfall directly impacts surface waters transported by the NECC. During this period of the year, the North Brazil Current retroflection transports the Amazon River plume waters into the NECC and towards the central tropical Atlantic, spatially overlapping with the zonal freshening caused by the ITCZ (Ibánhez et al., 2016). Lefèvre et al. (2020) recently identified the presence of the Amazon plume as far from the river mouth as at a mooring placed at 8°N 38°W. Our underway determinations were performed further East, at about 29°W along the 8°N latitudinal band. Although the distance between the mooring and the underway determinations presented here is still considerable, the significant CO_2 drawdown created by the spread of the Amazon plume could be spread further East contributing together with the ITCZ to the observed CO_2 undersaturation within the NECC. Finally, in the North of the study area (from ~9–10°N; Fig. 3), ΔfCO_2 reflects a marked seasonal pattern in the NEC. From November to March, the NEC is a net sink of atmospheric CO_2 (i.e. negative ΔfCO_2; Fig. 3, NOV-MAR) coinciding with the lower annual SST levels (Fig. 2, NOV-MAR), while it acts as a net source of CO_2 to the atmosphere from June to October (i.e. positive ΔfCO_2; Fig. 3, JUN-OCT).

3.2. ITCZ impact on the carbonate system in the tropical Atlantic

In the areas affected by recent rainfall and after removing the thermodynamic effect of SST over underway fCO_{2sw} (Eq. (8); hereafter termed $fCO_{2swnorm}$), we found robust, highly significant linear relationships of ln $fCO_{2swnorm}$ vs ln SSS ($r > 0.79$, n from 217 to 837) in 33 of the 35 ships' voyages analyzed here. These correspond to SSS gradients varying from 0.4 to

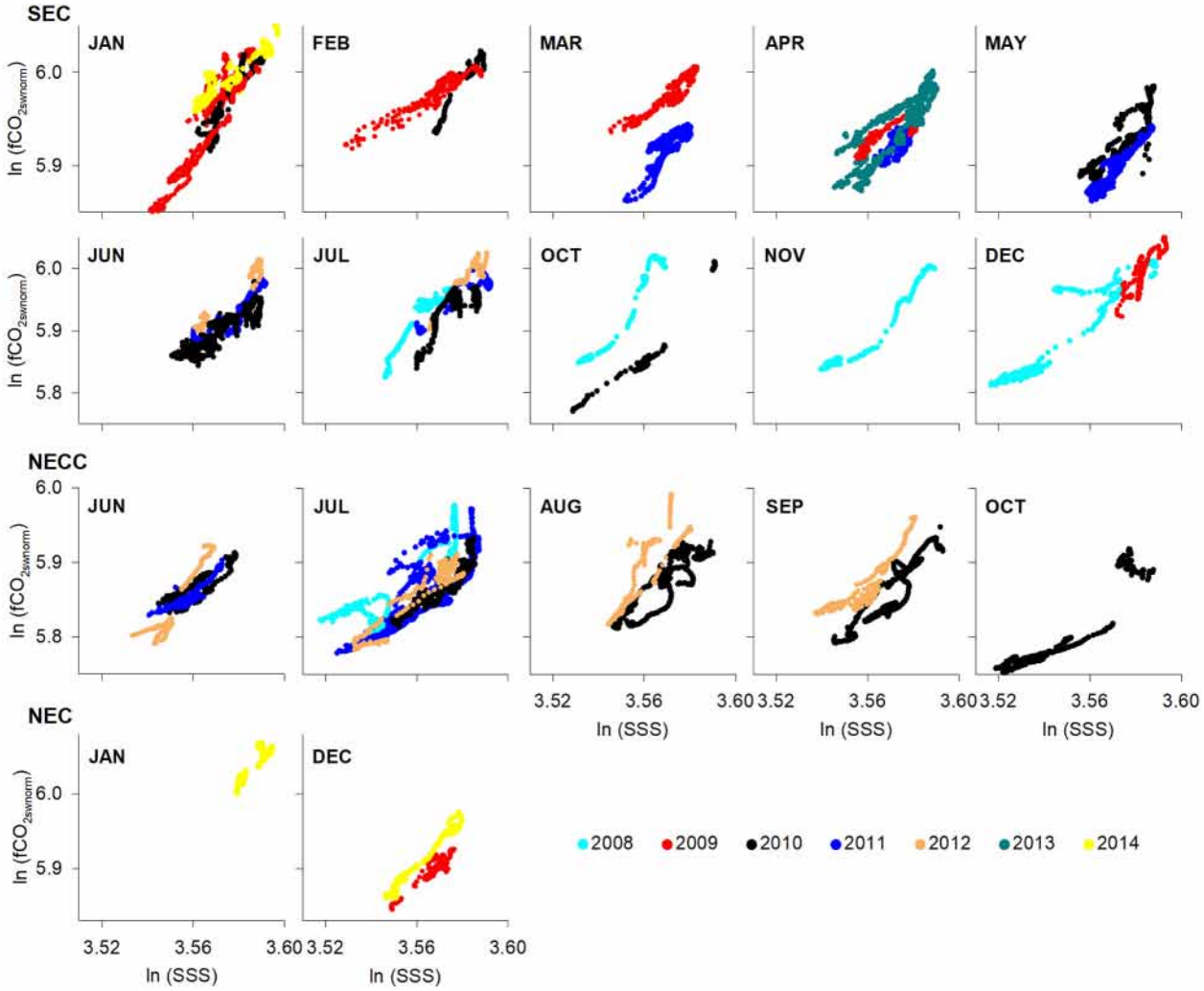

Fig. 4. Ln $fCO_{2swnorm}$ vs ln SSS constructed with the underway data with interpolated, short-term rainfall higher than 1 mm, discriminated by surface current (SEC, NECC, NEC) and month. Color code shown in the figure legend is used to indicate year. During January 2009, June 2010, July 2011 and April 2013, significant linear relationships of ln $fCO_{2swnorm}$ vs ln SSS were found in the northbound and southbound voyages.

2.5 salinity units and are found in the three main surface currents present in the study area (Table 2). Following the seasonal migration of the ITCZ, these significant linear relationships of ln $fCO_{2swnorm}$ vs ln SSS are found mainly in the SEC from December to May and in the NECC from June to November (Fig. 4). The overall thermodynamic effect of salinity changes caused by rainfall over fCO_{2sw}, γ_{rain}, calculated from these linear regressions (Eq. (9)), vary from 1.25 ± 0.04 to 4.98 ± 0.05, with an average value of 3.12. With the exception of γ_{rain} values obtained during the ships' voyages performed in February and April 2009, all the remaining γ_{rain} are well above the γ_{rain} reported from global means of the carbonate system sensitivity to rainfall at low latitudes (γ_{rain} = 1.6; Sarmiento and Gruber, 2006).

To evaluate the contribution of the different thermodynamic terms included in the overall γ_{rain}, we calculate the sensitivity of underway fCO_{2sw} to changes in TAlk (γ_{TAlk}) and DIC (γ_{DIC}) (Eqs. (10), (11)). Calculated γ_{DIC} and γ_{TAlk} are highly consistent among the different ships' voyages, ranging from 8.67 ± 0.00 to 9.19 ± 0.00 (γ_{DIC}) and −8.59 ± 0.00 to −8.09 ± 0.00 (γ_{TAlk}; Table 2). The resulting theoretical γ_{rain} calculated from γ_s, γ_{DIC} and γ_{TAlk} (Eq. (9)) remain systematically in the range of 1.58–1.60 (Table 2), i.e. the value proposed by Sarmiento and Gruber (2006) for low latitudes (1.6). These results suggest that the impact of the rainfall associated with the ITCZ over the surface water carbonate system in the tropical Atlantic cannot be explained solely by thermodynamics and chemical dilution of surface waters.

3.3. Sea-air CO_2 exchange in the tropical Atlantic affected by the ITCZ

Despite the lowering in fCO_{2sw} caused by rainfall, the areas affected by the ITCZ in the SEC were permanent sources of CO_2 to the atmosphere, ranging from 0.30 ± 0.01 to 3.31 ± 0.04 mmol m^{-2} d^{-1} (Table 3). This contrasts with the resulting sea-air CO_2 fluxes found in the areas affected by the ITCZ in the NECC and the NEC, which commonly acted as sinks of atmospheric CO_2. Nevertheless, the overall impact of the ITCZ over the sea-air CO_2 exchange in the tropical Atlantic is highly significant. CO_2 fluxes attributed to the impact of rainfall associated with the ITCZ range from −0.11 ± 0.01 mmol m^{-2} d^{-1} to −2.35 ± 0.08 mmol m^{-2} d^{-1} found in the SEC during May 2013 and in the NECC during August 2012,

Table 3
Sea-air CO_2 exchange affected by the ITCZ along the tracks of the vessels used in this study, discriminated by surface current in the tropical Atlantic. Sea-air CO_2 flux corresponds to that determined from underway measurements ($FCO_{2sea-air}$), ITCZ CO_2 drawdown (FCO_{2ITCZ}) corresponds to the calculated overall impact of the ITCZ over the sea-air CO_2 exchange, while unexplained CO_2 flux corresponds to that not explained by thermodynamics ($FCO_{2unknown}$). The significant negative correlations between MODIS/aqua, monthly Chl *a* and measured SSS and fCO_{2sw} normalized to temperature ($fCO_{2swnorm}$) are also shown, together with the number of interpolated Chl *a* values used (n Chl. *a*). ID corresponds to the identification of each VOS voyage used in Table 1. p-value is indicated with the following code: *** p < 0.0001, ** p < 0.001, * p < 0.01, while absence of code indicates p < 0.05. No significant (p > 0.05) Chl. *a* vs SSS and Chl. *a* vs $fCO_{2swnorm}$ relationships are denoted by empty fields.

ID	Month	Year	Current	$FCO_{2sea-air}$ mmol m^{-2} d^{-1}	FCO_{2ITCZ} mmol m^{-2} d^{-1}	$FCO_{2unknown}$ mmol m^{-2} d^{-1}	n FCO_2	Chl. *a* vs SSS (r)	Chl. *a* vs $fCO_{2swnorm}$ (r)	n Chl. *a*
1	7	2008	SEC	0.81 ± 0.03	−1.30 ± 0.02	−0.84 ± 0.01	558	−0.60***	−0.63***	512
			NECC	0.14 ± 0.06	−1.06 ± 0.06	−0.60 ± 0.04	412			
2	10	2008	SEC	1.54 ± 0.09	−1.52 ± 0.07	−1.17 ± 0.05	289	−0.42***	−0.33***	108
3	11	2008	SEC	0.78 ± 0.05	−1.02 ± 0.04	−0.56 ± 0.03	360	−0.26***	−0.26***	224
4	12	2008	SEC	1.05 ± 0.05	−0.43 ± 0.02	−0.24 ± 0.01	427	−0.59***	−0.47***	202
5	1	2009	SEC	0.96 ± 0.07	−1.64 ± 0.04	−0.99 ± 0.03	353	−0.70***	−0.72***	138
6	1	2009	SEC	2.11 ± 0.06	−1.60 ± 0.09	−1.51 ± 0.05	687	−0.62***		336
7	2	2009	SEC	0.99 ± 0.05	−0.26 ± 0.01	0.00 ± 0.00	494	−0.82***	−0.73***	180
8	3	2009	SEC	1.98 ± 0.03	−0.44 ± 0.02	−0.08 ± 0.01	427		−0.15	225
9	4	2009	SEC	0.75 ± 0.01	−0.16 ± 0.01	0.00 ± 0.01	368			
10	12	2009	SEC	3.31 ± 0.04	−1.32 ± 0.04	−0.89 ± 0.03	572	−0.85***	−0.81***	145
			NEC	−0.44 ± 0.03	−0.67 ± 0.03	−0.30 ± 0.01	283			
11	1	2010	SEC	1.60 ± 0.05	−0.63 ± 0.02	−0.34 ± 0.01	440	−0.77***	−0.81***	163
12	2	2010	SEC	0.86 ± 0.01	−0.30 ± 0.02	−0.17 ± 0.01	318		0.21*	191
15	5	2010	SEC	1.57 ± 0.06	−0.63 ± 0.04	−0.25 ± 0.02	712	−0.66***	−0.72***	566
16	6	2010	SEC	0.84 ± 0.03	−0.28 ± 0.01	−0.11 ± 0.01	806	−0.38***	−0.27***	616
17	6	2010	SEC	2.23 ± 0.06	−0.60 ± 0.03	−0.30 ± 0.02	619	−0.65***	−0.60***	503
			NECC	0.05 ± 0.01	−0.42 ± 0.02	−0.12 ± 0.01	360	−0.54***	−0.22*	188
18	7	2010	SEC	1.84 ± 0.04	−1.16 ± 0.03	−0.56 ± 0.03	594	−0.66***	−0.62***	560
			NECC	0.12 ± 0.01	−0.30 ± 0.01	−0.11 ± 0.00	697			
19	8	2010	NECC	0.21 ± 0.05	−1.98 ± 0.05	−0.80 ± 0.03	670			
20	9	2010	NECC	−0.20 ± 0.05	−1.95 ± 0.04	−0.90 ± 0.02	636	−0.14		200
21	10	2010	SEC	0.51 ± 0.08	−2.28 ± 0.08	−1.38 ± 0.06	305	−0.67***	−0.55***	129
			NECC	−0.38 ± 0.06	−1.97 ± 0.06	−0.69 ± 0.03	500	−0.23***		417
22	3	2011	SEC	1.71 ± 0.04	−0.56 ± 0.02	−0.17 ± 0.01	830	−0.77***	−0.53***	379
23	4	2011	SEC	0.81 ± 0.02	−0.31 ± 0.01	−0.10 ± 0.01	464	−0.14	−0.43***	282
24	5	2011	SEC	0.30 ± 0.01	−0.88 ± 0.03	−0.39 ± 0.01	837	−0.57***	−0.54***	704
25	6	2011	SEC	1.60 ± 0.02	−1.07 ± 0.04	−0.49 ± 0.03	445			
			NECC	0.00 ± 0.02	−0.45 ± 0.01	−0.11 ± 0.01	242	−0.36***	−0.49***	119
26	7	2011	NECC	0.00 ± 0.01	−0.27 ± 0.01	−0.09 ± 0.01	473	−0.62***	−0.30***	226
27	7	2011	SEC	1.39 ± 0.03	−0.92 ± 0.06	−0.33 ± 0.03	303	−0.41***		258
			NECC	−0.31 ± 0.03	−1.49 ± 0.04	−0.75 ± 0.03	481			
28	6	2012	SEC	3.19 ± 0.09	−1.54 ± 0.06	−0.84 ± 0.04	482	−0.55***	−0.56***	438
			NECC	−0.51 ± 0.04	−0.93 ± 0.04	−0.59 ± 0.02	217			
29	7	2012	SEC	2.11 ± 0.08	−1.07 ± 0.04	−0.68 ± 0.03	383			
			NECC	−0.42 ± 0.01	−0.37 ± 0.02	−0.13 ± 0.01	372			
30	8	2012	NECC	−0.92 ± 0.07	−2.35 ± 0.08	−1.45 ± 0.06	293			
31	9	2012	NECC	−0.16 ± 0.02	−0.56 ± 0.02	−0.23 ± 0.01	386	−0.51***		233
32	4	2013	SEC	1.24 ± 0.04	−0.30 ± 0.04	−0.31 ± 0.02	515			
33	4	2013	SEC	1.62 ± 0.04	−0.11 ± 0.02	−0.28 ± 0.01	585	−0.46***	−0.49***	452
34	1	2014	SEC	0.91 ± 0.03	−0.29 ± 0.01	−0.06 ± 0.06	498	−0.76***	−0.78***	372
			NEC	−0.72 ± 0.07	−1.02 ± 0.04	−0.65 ± 0.03	285			
35	12	2014	SEC	2.75 ± 0.08	−0.77 ± 0.02	−0.47 ± 0.02	389			
			NEC	−0.16 ± 0.02	−0.29 ± 0.02	−0.22 ± 0.01	401			

respectively. Despite the increase in the gas transfer caused by rainfall, the ITCZ significantly lowers CO_2 outgassing in the region (Table 3).

The imbalance among the observed fCO_{2sw} change caused by the freshening associated with rainfall in the area and that expected from thermodynamics alone showed previously also promotes an unexplained lowering of the sea-air CO_2 exchange in the area (hereafter termed CO_2 drawdown). This unexplained CO_2 drawdown ($FCO_{2unknown}$) results to be generally of higher magnitude than that expected from thermodynamics alone, ranging from 0.00 ± 0.00 to −1.38 ± 0.06 mmol m^{-2} d^{-1} (Table 3). Only two areas (SEC in February and April 2009) show a small positive CO_2 flux imbalance explained by the observed γ_{rain} slightly lower than the thermodynamic value of 1.6 (Table 2). Despite the variable γ_{rain} found in this study and the impact of the variable wind speed over the calculated sea-air CO_2 fluxes, there is a highly significant correlation among the total (FCO_{2ITCZ}) and the unexplained CO_2 drawdown ($FCO_{2unknown}$) associated with the ITCZ (R = 0.91; Fig. 5). Taking this linear relationship, the unexplained portion of the sea-air CO_2 exchange in the areas affected by the ITCZ represents on average 59.1 ± 4.1 % of the total observed CO_2 drawdown.

After normalization of measured fCO_{2sw} to SST (i.e. removal of fCO_{2sw} changes promoted by SST changes), abiotic factors (SSS changes and DIC and TAlk dilution caused by rainfall) only explain ~41 % of the calculated CO_2 drawdown in the surface waters of the tropical Atlantic associated with the ITCZ. MODIS/aqua, monthly Chl *a* concentration along the tracks used here shows a distinctive distribution within the areas affected by recent rainfall. Despite the large cloud coverage in the area which makes remote-sensed Chl *a* estimations unavailable in some areas and precluded comparison of daily Chl *a* data with underway measurements, we find significant negative correlations between monthly Chl *a* and underway SSS in the majority of the areas where we found robust ln SSS vs ln $fCO_{2swnorm}$ relationships (Table 3). Similarly, monthly Chl *a* was also negatively correlated with $fCO_{2swnorm}$.

4. Discussion

4.1. Enhanced CO_2 drawdown in the tropical Atlantic affected by the ITCZ

Nitrogen availability is commonly found as the limiting nutrient for primary producers' growth in low-latitude, stratified oceans such as the tropical Atlantic (Moore et al., 2013). In the Pacific Ocean, Hansell and Feely (2000) hypothesize that increased stratification forced by rainfall associated with the ITCZ, which further limits the transport of N from the deeper layers to the surface, enhances N_2 fixation in these areas due to the competitive advantage of diazotrophs under N-depleted conditions. This increases organic C and N concentrations in the surface waters and lowers surface

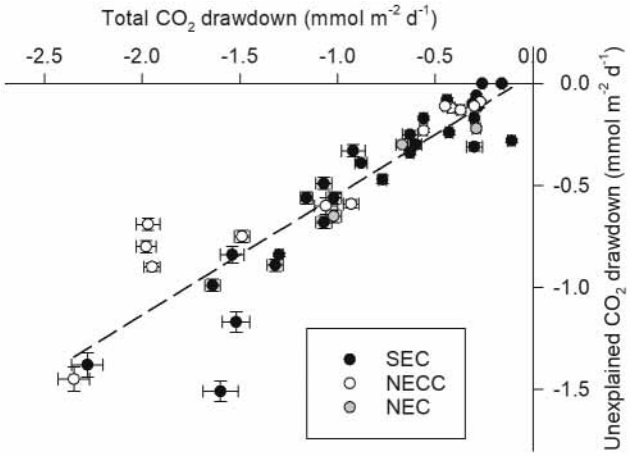

Fig. 5. Correlation of the atmospheric CO_2 drawdown attributed to the impact of the ITCZ in the tropical Atlantic (FCO_{2ITCZ}) and that unexplained by the physical and thermodynamic processes caused by rainfall, $FCO_{2unknown}$ (i.e. turbulent sea-air CO_2 exchange, SSS change, dilution of TA and DIC).

fCO_{2sw} (Hansell and Feely, 2000), adding to the lowering of fCO_{2sw} caused by rainfall dilution in the tropical Pacific (Ho and Schanze, 2020). Widespread high abundances of *Trichodesmium* are found across the tropical Atlantic basin (Benavides and Voss, 2015 and references therein), with the highest abundances in between 5°S and 15°N (Fernández et al., 2010; Moore et al., 2009; Schlosser et al., 2014). Adding to the widespread dominance of *Trichodesmium* across the tropical Atlantic, diatom-diazotroph associations are abundant in the outer plume areas fuelled by the phosphate and silicate excess after nitrate exhaustion transported from land (Subramaniam et al., 2008, 2013), while unicellular diazotrophic cyanobacteria are also abundant in the equatorial upwelling area (Foster et al., 2009). Mulholland and Capone (2001) report a CO_2:N_2 stoichiometric utilization ratio of 28 in cultured populations of *Trichodesmium* IMS101. Assuming this CO_2:N_2 stoichiometric utilization ratio for the natural diazotroph populations of the tropical Atlantic, the unexplained CO_2 drawdown identified here in the zones affected by the ITCZ (excluding the two γ_{rain} values lower than the thermodynamic value) would represent N_2 fixation ratios ranging from 2.2 ± 0.2 to 53.9 ± 1.9 μmol m^{-2} d^{-1}, with a median value of 13.0 μmol m^{-2} d^{-1}. These potential N_2 fixation ratios calculated are well within the range of values previously measured in the studied area. Fernández et al. (2010) reports averaged N_2 fixation ratios in the equatorial region of 66 and 55 μmol m^{-2} d^{-1} during two campaigns in 2007 and 2008, while other studies report values well exceeding 100 μmol m^{-2} d^{-1} in the region (Schlosser et al., 2014; Subramaniam et al., 2013).

The highly significant linear dependency of ln fCO_{2sw} with ln SSS together with the negative relationship of Chl *a* with SSS and fCO_{2sw} found in most of the areas affected by the ITCZ in the VOS used here suggest a direct link between the ITCZ and primary production in the central tropical Atlantic. The tropical and subtropical North Atlantic receives the largest fluxes of continental dust of all oceans originated from northwest Africa (Mahowald et al., 2009) that cross the basin reaching the Caribbean Sea and America (Prospero et al., 2014). When reaching the ITCZ area, these atmospheric particles are washed out and deposited in the surface waters, thus fertilizing the oligotrophic tropical Atlantic (Baker et al., 2007; Fernández et al., 2010; Schlosser et al., 2014).

In the study area, wet dust deposition is the main pathway of entrance of Saharan and Sahel dust to surface waters, exceeding in one order of magnitude the amount of dry dust deposition in the area and strongly associated with the ITCZ (Fig. 6). Throughout the studied period (2008–2014), the monthly latitudinal maximum wet dust deposition in the study area is permanently North to the ITCZ and following its seasonal migration as expected (Figs. 1, 7b). Nevertheless, both rainfall and wet dust deposition show significant interannual variability in the study area (Fig. 7b). Particularly notorious is the prolonged negative rainfall anomaly registered during late 2009 and early 2010. These were years of significant climatic anomalies in the tropical Atlantic, following the Pacific El Niño of 2009 (Ibánhez et al., 2017; Lefèvre et al., 2013, 2019). During late 2008-early 2009, a positive anomaly in rainfall intensity is verified concomitant with a positive anomaly of wet dust deposition (Fig. 7b) and associated with a La Niña Modoki event in 2008 (Tyaquiçã et al., 2017). Afterwards, a shift in the position of the ITCZ towards North during late 2009 (Fig. 7a) is accompanied by the most negative rainfall intensity anomalies of the time series analyzed here, that lasted until April 2010 (Fig. 7b). Furthermore, the only two ships' voyages where we didn't find significant linear relationships of ln SSS vs ln fCO_{2sw} correspond to March 2010, when the ITCZ showed an anomalous northward shift remaining North of the SEC (Lefèvre et al., 2013). The highest CO_2 drawdown associated with the ITCZ are registered during early 2009, late 2010 and 2012 (Fig. 7b). Similar events to that registered during 2009 associated with a Pacific La Niña phase are also registered during 2012 and 2014, affecting both the position and intensity of rainfall associated with the ITCZ, although these are not associated with wind and SST anomalies as in 2009 (Tyaquiçã et al., 2017). Nevertheless, and rather than associated with rainfall intensity anomalies in the study area, calculated CO_2 drawdown associated with the ITCZ showed significant correlation with monthly wet dust deposition anomalies in the SEC

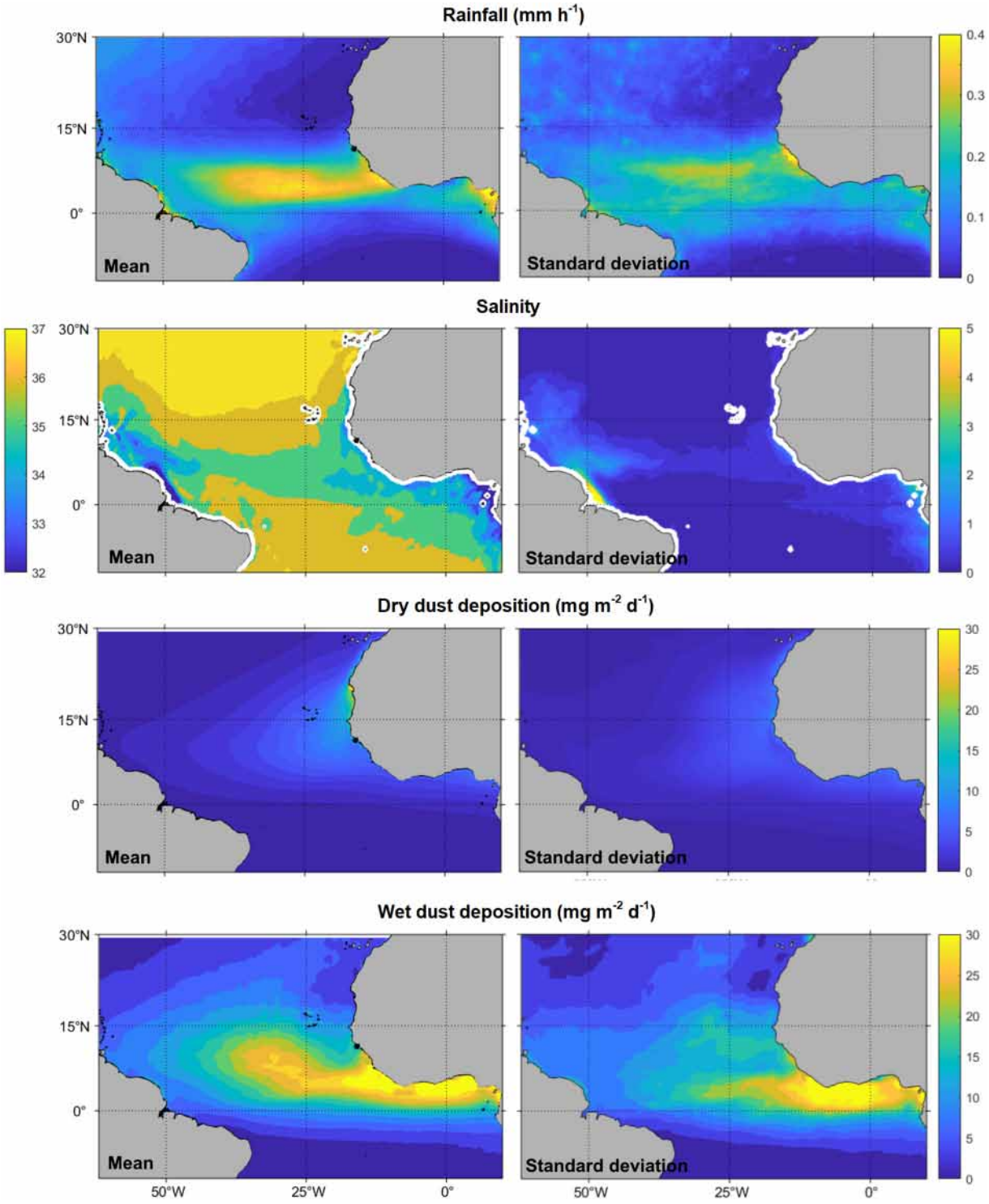

Fig. 6. Long-term mean and standard deviation of rainfall, sea surface salinity, dry dust deposition and wet dust deposition in the central tropical Atlantic. Data correspond to the average of monthly data from 1998 until 2014, except for the salinity data that include the period 2011 to 2014.

(i.e. higher CO_2 drawdown during positive wet dust deposition anomalies; $\rho = 0.41$; $p < 0.05$; $n = 28$). Together with the significant correlations found between monthly Chl *a* and underway data despite the temporal scale mismatch of these datasets (monthly to underway), these relationships suggest a spatially and temporally sustained impact of the ITCZ over the primary production and carbonate system of the tropical Atlantic. Extrapolating our underway measurements to the monthly scale, monthly-averaged CO_2 drawdown associated with the ITCZ, calculated using the monthly-averaged wind and rainfall fields, showed also significant correlation with monthly wet dust deposition anomalies ($\rho = 0.35$; $p < 0.02$; $n = 44$; Fig. 7b).

Compared to dry dust deposition, wet dust deposition favors nutrient leaching due to the low pH of rainfall and the presence of chelating ligands (Johnson and Meskhidze, 2013; Meskhidze et al., 2005). The drop in SSS caused by rainfall further develops a strong pycnocline creating a barrier layer that limit vertical mixture and exchange of solutes (Mignot et al., 2012), limiting the availability of these solutes to the upper part of the ocean. Schlosser et al. (2014) found iron concentrations in the central

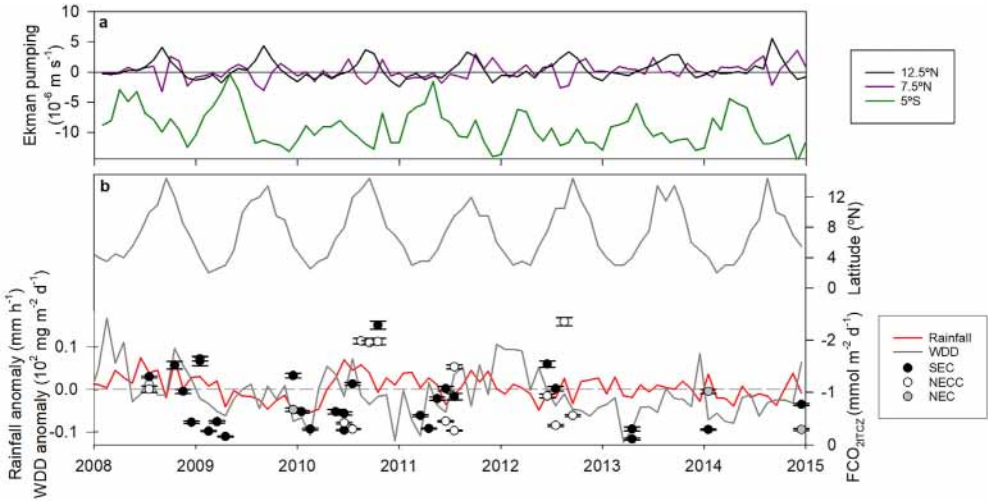

Fig. 7. a. Monthly-averaged Ekman pumping calculated at 5°S, 7.5°N and 12.5°N and integrated over the 18–36°W longitudinal band. Positive values denote upwelling. b. Monthly latitudinal maximum wet dust deposition (WDD; grey line) calculated as the monthly maximum precipitation latitudinal band within 5°S–15°N and averaged for the 18–36°W longitudinal band. The monthly rainfall (red line) and wet dust deposition (grey line) anomalies in the central tropical Atlantic (5°S–15°N and 18–36°W) together with the calculated monthly CO_2 drawdown caused by the ITCZ (FCO_{2ITCZ}) discriminated by oceanic surface currents (South Equatorial Current, SEC; North Equatorial Current, NEC; North Equatorial Countercurrent, NECC) are also shown.

tropical Atlantic that almost perfectly matched the distribution of the freshening caused by the ITCZ and hence, diazotrophy rates. *Trichodesmium* and other diazotrophs are generally limited by iron availability due to the high iron cost of the nitrogenase enzyme (Kustka et al., 2002). Short-term diazotrophy enhancement has been linked to wet dust deposition by the ITCZ in the tropical Atlantic (Fernández et al., 2010; Schlosser et al., 2014). Furthermore, wet dust deposition can also transport large amounts of both organic and inorganic P and N to surface waters of the tropical Atlantic (Baker et al., 2007; Zamora et al., 2013). Baker et al. (2007) found that wet deposition could introduce atmospheric, bioavailable inorganic N that could rival the amount of N fixed in the tropical Atlantic, thus supporting primary production other than diazotrophy and directly associated with the ITCZ. Indeed, the spatial mismatch between the ITCZ and the transport of nutrients through wet dust deposition, placed to the North of the ITCZ (Fig. 1; Fig. 7b), may explain the systematic nonlinearities observed in the ln SSS vs ln $fCO_{2swnorm}$ found (Fig. 4). Despite the high correlations found, ln SSS vs ln $fCO_{2swnorm}$ commonly shows steeper slopes (i.e. higher deviations from the expected thermodynamic γ_{rain}) at higher ln SSS (i.e. lower dilution by rainfall). This is consistent with higher wet dust deposition at the northern edge of the ITCZ. This is particularly observable in the SEC during October and November and in the NECC during July and September (Fig. 4).

Other processes could partially explain the increased Chl *a* associated with the drop in SSS observed and, hence, the enhanced CO_2 drawdown linked to the freshening of the central tropical Atlantic. The seasonal migration of the ITCZ drives the seasonality of wind forcing and related Ekman transport that feeds the surface and subsurface system of currents (Castellanos et al., 2015). Despite that the Coriolis term is small near the equator, significant vertical Ekman transport are calculated for the 5°S, 7.5°N and 12.5°N, representative of the SEC, NECC and NEC areas, respectively (Fig. 7a). Downwelling prevails year round in the SEC area. In the NECC and NEC areas, seasonal pulses of upwelling are verified following the migration of the ITCZ (Fig. 1). Subsurface waters, richer in nutrients and CO_2, could partially feed primary production in surface waters (Table 4). Nevertheless, no significant increase in CO_2 is observed in the areas affected by the ITCZ (Bruto et al., 2017) and thus, vertical Ekman transport may not be the main contributor to the observed enhanced Chl *a* in the areas affected by the freshening caused by the ITCZ.

The overlapping of the freshening caused by the ITCZ with the seasonal spread of the Amazon plume by the NECC (Ibánhez et al., 2016) could also drive to misinterpretation of our results in the NECC region. The TAlk vs SSS relationship used to calculate the thermodynamic γ_{rain} together with measured fCO_2 levels includes both samples taken in the area of influence of the ITCZ and the Amazon River plume (Lefèvre et al., 2010). Thus, our approach to verify the deviation from thermodynamics in the freshening area would also be valid if that would be caused by the Amazon River plume. Using the highly significant linear relationship of fCO_2 with SSS in the outer Amazon River plume ($r = 0.9$; $n = 6393$) presented in Ibánhez

Table 4
Summary of the main known and potential effects of processes directly related to the Atlantic ITCZ over the carbonate system of surface waters.

Process	Driver	Effects over the sea surface carbonate system	
Enhanced gas transfer	Turbulence caused by rain drops	Increase the magnitude of sea-air CO_2 exchange	Harrison et al. (2012), Ho et al. (2000)
Change in SSS and SST	Rainfall	Change in carbonate system equilibrium constants, CO_2 solubility, …	e.g. Weiss (1974), Takahashi et al. (2009), Sarmiento and Gruber (2006)
Dilution	Rainfall	Lowering TAlk and DIC	Ashton et al. (2016), Ho and Schanze (2020), Turk et al. (2010), Woolf et al. (2019)
Wet deposition of DIC	Rainfall	Transport of atmospheric CO_2 into surface waters	Turk et al. (2010)
Formation of barrier layers	Rainfall	Limiting vertical exchange of carbonate system properties	e.g. Mignot et al. (2012)
Ekman transport	Wind	Downwelling of surface waters, upwelling of deep waters, change in carbonate system properties and primary producers' growth	e.g. Castellanos et al. (2015)
Fertilization	Rainfall	Wet deposition of dust and atmospheric N and P driving the consumption of CO_2 by primary producers' growth	e.g. Baker et al. (2007), Fernández et al. (2010), Schlosser et al. (2014)

et al. (2015), the overall effect of salinity changes caused by the plume over fCO_{2sw} is 1.67 ± 0.06. This is higher than that expected from thermodynamics alone (1.6) but still significantly smaller than those found in the area of influence of the ITCZ in the NECC. Although a contribution of Amazon plume waters to the observed freshening and CO_2 drawdown in the area of influence of the ITCZ cannot be disregarded, it cannot explain the enhanced CO2 drawdown observed. Thus, the ITCZ seems able to support primary production in the otherwise oligotrophic tropical Atlantic that could explain the enhanced linear ln SSS vs ln $fCO_{2swnorm}$ relationships and atmospheric CO_2 drawdown found in this study.

4.2. The Atlantic ITCZ in the global oceanic CO_2 sink

The underway fCO_{2sw} data used in this study were collected by VOS as part of current fCO_{2sw} monitoring programs. As shown by Ho and Schanze (2020) in the tropical Pacific, rainfall impacts over the ocean chemistry can be restricted to a narrow surface layer, often missed by underway VOS determinations due to the deep intake port of these ships (3–5 m deep). Despite this limitation, the freshening caused by the ITCZ in the tropical Atlantic was clearly recorded by the underway determinations used here. A vertical gradient of the impact of the ITCZ over the surface ocean chemistry would nevertheless likely exist and therefore, the dilution of carbonate system parameters of surface waters caused by the Atlantic ITCZ may be much larger than that shown here. As this dilution causes a lowering of fCO_{2sw} and thus, a lowering of sea surface CO_2 outgassing in oversaturated areas and an increase of the oceanic CO_2 sink in undersaturated areas (Table 4), our findings can be taken as a conservative estimation of the impact of the ITCZ over the sea-air CO_2 exchange in the tropical Atlantic.

Ashton et al. (2016) estimate that up to 6 % of the global oceanic CO_2 sink is caused by rainfall over the ocean surface. As they used extensive underway fCO_{2sw} measurements, the effect of rainfall over the sea surface carbonate system is already accounted in their estimations but not directly attributed to rainfall. This has strong implications on our understanding of the global oceanic CO_2 exchange, as changes in the global precipitation regime would promote unquantified changes in the global oceanic CO_2 sink. Turk et al. (2010) estimated the overall contribution of rainfall to the sea-air CO_2 exchange in the western equatorial Pacific by including also the dilution effect. They found that the region changes from a source to a sink of atmospheric CO_2 caused by this dilution effect and subsequent lowering of fCO_{2sw}. Adding to the physical and thermodynamic effects of rainfall over the oceanic surface carbonate system and sea-air CO_2 exchange, we show evidence for the enhanced CO_2 drawdown associated with the ITCZ in the tropical Atlantic. Fertilization driven by the ITCZ seems to promote primary production that, in turn, significantly reduces CO_2 emissions to the atmosphere in the oligotrophic tropical Atlantic. A large zonal gradient of this enhancement is expected due to the large East-to-West gradient of wet dust deposition fluxes, together with the spatial overlapping with the zonal spread of large river plumes at the edges of the basin (Ibánhez et al., 2016; Körtzinger, 2010; Lefèvre, 2009). Thus, extrapolations of our findings at the basin scale should be made with caution. Nevertheless, our results suggest that the combined effects of the ITCZ over the sea-air CO_2 budget significantly reduce oceanic CO_2 emissions to the atmosphere in the tropical Atlantic.

Climate models project a weaker, narrower ITCZ due to anthropogenic warming (Byrne and Schneider, 2016b,a), adding to the impact of interannual climate modes over the rainfall regime of the tropical Atlantic (Lübbecke et al., 2018; Richter and Tokinaga, 2021). Increasing CO_2 outgassing caused by rising SST in the tropical Atlantic (Servain et al., 2014; Ibánhez et al., 2017; Lefèvre et al., 2019), would act together with the projected changes in the Atlantic ITCZ to further reduce the overall oceanic mitigation of anthropogenic CO_2 emissions to the atmosphere. Nevertheless, the interannual variability of sea-air CO_2 exchange and the impact of these projected changes over the CO_2 budget of the tropical Atlantic are poorly understood.

5. Conclusions

Through the analysis of extensive underway data collected by voluntary merchant ships in the tropical Atlantic, we show the large impact of the freshening caused by the ITCZ on the carbonate system of the basin. Freshening associated with the ITCZ dilutes fCO_{2sw} thus reducing the magnitude of CO_2 outgassing in the area. Nevertheless, we have performed a thermodynamic analysis of the changes in fCO_{2sw} associated with SSS changes promoted by the ITCZ and found that physics and thermodynamics alone cannot explain the magnitude of the observed CO_2 drawdown. Instead, the freshening caused by the ITCZ appears associated to an increase in Chl *a* in surface waters of the oligotrophic tropical Atlantic. The particularities of the Atlantic ITCZ compared to the other tropical oceanic basins, such as the presence of the Amazon River plume and the input of dust originated from the Sahara and the Sahel may explain the observed enhanced CO_2 drawdown demonstrated here. The ITCZ serves as a North to South divide in the transport of continental dust and enhances the deposition of continental material in surface waters. These, in turn, fertilize the oligotrophic tropical Atlantic and seem to be the main mechanism explaining the large CO_2 drawdown caused by the ITCZ. As shown in this study, regular fCO_{2sw} monitoring programs provide excellent means to disentangle the processes affecting sea-air CO_2 exchange at large spatial and temporal scales.

Credit authorship contribution statement

JSPI: Funding acquisition, Conceptualization, Formal Analysis, Writing – original draft. MF: Funding acquisition, Writing – review & editing. NL: Funding acquisition, Data curation, Resources, Writing – review & editing.

Declaration of competing interest

The authors declare the following financial interests/personal relationships which may be considered as potential competing interests: Severino Ibanhez reports financial support was provided by Irish Research Council. Severino Ibanhez reports financial support was provided by European Commission. Nathalie Lefevre reports financial support was provided by European Commission. Manuel Flores reports financial support was provided by CAPES.

Acknowledgements

This research was financed by the European Integrated Projects CARBOOCEAN (contract 511176–2) and CARBOCHANGE (FP7 264879), Atlantos (grant agreement 633211), the DICAM project (CAPES CM II 1975/2014) and the Institut de Recherche pour le Développement (IRD). Data analysis and manuscript preparation was further financed by the SUB-ACID project, funded by the Irish Research Council and the European Union's Horizon 2020 research and innovation programme under the Marie Skłodowska-Curie grant agreement No 713279 through the CAROLINE program (CLNE/2017/210). The underway data used in this study is publicly accessible in the SOCAT (https://www.socat.info) and SEANOE (https://www.seanoe.org) databases. We thank the comments of three anonymous reviewers.

Appendix A. Supplementary data

Supplementary data to this article can be found online at https://doi.org/10.1016/j.scitotenv.2022.156592.

References

Andrié, C., Oudot, C., Genthon, C., Merlivat, L., 1986. CO2 fluxes in the tropical Atlantic during FOCAL cruises. J. Geophys. Res. Oceans 91 (C10), 11741–11755. https://doi.org/10.1029/JC091iC10p11741.

Ashton, I.G., Shutler, J.D., Land, P.E., Woolf, D.K., Quartly, G.D., 2016. A sensitivity analysis of the impact of rain on regional and global sea-air fluxes of CO 2. PLoS ONE 11 (9), e0161105. https://doi.org/10.1371/journal.pone.0161105.

Baker, A.R., Weston, K., Kelly, S.D., Voss, M., Streu, P., Cape, J.N., 2007. Dry and wet deposition of nutrients from the tropical Atlantic atmosphere: links to primary productivity and nitrogen fixation. Deep-Sea Res. I Oceanogr. Res. Pap. 54 (10), 1704–1720. https://doi.org/10.1016/j.dsr.2007.07.001.

Benavides, M., Voss, M., 2015. Five decades of N2 fixation research in the North Atlantic Ocean. Mar. Biogeochem. 2, 40. https://doi.org/10.3389/fmars.2015.00040.

Bianchi, T.S., Allison, M.A., 2009. Large-river delta-front estuaries as natural "recorders" of global environmental change. Proc. Natl. Acad. Sci. 106 (20), 8085–8092. https://doi.org/10.1073/pnas.0812878106.

Bourlès, B., Araujo, M., McPhaden, M.J., Brandt, P., Foltz, G.R., Lumpkin, R., et al., 2019. PIRATA: a sustained observing system for tropical Atlantic climate research and forecasting. Earth Space Sci. 6, 577–616. https://doi.org/10.1029/2018EA000428.

Boutin, J., Chao, Y., Asher, W.E., Delcroix, T., Drucker, R., Drushka, K., et al., 2015. Satellite and in situ salinity: understanding near-surface stratification and subfootprint variability. Bull. Am. Meteorol. Soc. 97 (8), 1391–1407. https://doi.org/10.1175/BAMS-D-15-00032.1.

Bruto, L., Araujo, M., Noriega, C., Veleda, D., Lefèvre, N., 2017. Variability of CO2 fugacity at the western edge of the tropical Atlantic Ocean from the 8°N − 38°W PIRATA buoy. Dyn. Atmos. Oceans 78, 1–13. https://doi.org/10.1016/j.dynatmoce.2017.01.003.

Byrne, M.P., Schneider, T., 2016a. Energetic constraints on the width of the intertropical convergence zone. J. Clim. 29 (13), 4709–4721. https://doi.org/10.1175/JCLI-D-15-0767.1.

Byrne, M.P., Schneider, T., 2016b. Narrowing of the ITCZ in a warming climate: physical mechanisms. Geophys. Res. Lett. 43 (21), 11,350–11,357. https://doi.org/10.1002/2016GL070396.

Castellanos, P., Pelegrí, J.L., Campos, E.J.D., Rosell-Fieschi, M., Gasser, M., 2015. Response of the surface tropical Atlantic Ocean to wind forcing. Prog. Oceanogr. 134, 271–292. https://doi.org/10.1016/j.pocean.2015.02.005.

Cooley, S.R., Coles, V.J., Subramaniam, A., Yager, P.L., 2007. Seasonal variations in the Amazon plume-related atmospheric carbon sink. Glob. Biogeochem. Cycles 21 (3), GB3014. https://doi.org/10.1029/2006GB002831.

Dessier, A., Donguy, J.R., 1994. The sea surface salinity in the tropical Atlantic between 10°S and 30°N—seasonal and interannual variations (1977–1989). Deep-Sea Res. I Oceanogr. Res. Pap. 41 (1), 81–100. https://doi.org/10.1016/0967-0637(94)90027-2.

Dickson, A.G., Millero, F.J., 1987. A comparison of the equilibrium constants for the dissociation of carbonic acid in seawater media. Deep Sea Res. Part A Oceanogr. Res. Pap. 34 (10), 1733–1743. https://doi.org/10.1016/0198-0149(87)90021-5.

Dickson, A.G., Sabine, C.L., Christian, J.R., 2007. Guide to Best Practices for Ocean CO2 Measurements. (Report). North Pacific Marine Science Organization Retrieved from http://www.oceandatapractices.net:80/handle/11329/249.

van der Does, M., Brummer, G.-J.A., van Crimpen, F.C.J., Korte, L.F., Mahowald, N.M., Merkel, U., et al., 2020. Tropical rains controlling deposition of Saharan dust across the North Atlantic Ocean. Geophys. Res. Lett. 47 (5). https://doi.org/10.1029/2019GL086867 e2019GL086867.

Donohoe, A., Marshall, J., Ferreira, D., Mcgee, D., 2013. The relationship between ITCZ location and cross-equatorial atmospheric heat transport: from the seasonal cycle to the last glacial maximum. J. Clim. 26 (11), 3597–3618. https://doi.org/10.1175/JCLI-D-12-00467.1.

Fernández, A., Mouriño-Carballido, B., Bode, A., Varela, M., Marañón, E., 2010. Latitudinal distribution of Trichodesmium spp. and N2 fixation in the Atlantic Ocean. Biogeosciences 7 (10), 3167–3176. https://doi.org/10.5194/bg-7-3167-2010.

Fonseca, C.A., Goni, G.J., Johns, W.E., Campos, E.J.D., 2004. Investigation of the North Brazil current retroflection and North Equatorial Countercurrent variability. Geophys. Res. Lett. 31 (21), L21304. https://doi.org/10.1029/2004GL020054.

Foster, R.A., Subramaniam, A., Zehr, J.P., 2009. Distribution and activity of diazotrophs in the Eastern Equatorial Atlantic. Environ. Microbiol. 11 (4), 741–750. https://doi.org/10.1111/j.1462-2920.2008.01796.x.

Friedlingstein, P., O'Sullivan, M., Jones, M.W., Andrew, R.M., Hauck, J., Olsen, A., et al., 2020. Global carbon budget 2020. Earth Syst. Sci. Data 12 (4), 3269–3340. https://doi.org/10.5194/essd-12-3269-2020.

Gelaro, R., McCarty, W., Suárez, M.J., Todling, R., Molod, A., Takacs, L., et al., 2017. The modern-era retrospective analysis for research and applications, version 2 (MERRA-2). J. Clim. 30 (14), 5419–5454. https://doi.org/10.1175/JCLI-D-16-0758.1.

Grodsky, S.A., Reul, N., Vandemark, D., Bentamy, A., 2020. Intramonth oscillations of Atlantic ITCZ observed in SMAP satellite salinity. Int. J. Remote Sens. 41 (3), 839–857. https://doi.org/10.1080/01431161.2019.1648908.

Hansell, D.A., Feely, R.A., 2000. Atmospheric Intertropical Convergence impacts surface ocean carbon and nitrogen biogeochemistry in the western tropical Pacific. Geophys. Res. Lett. 27 (7), 1013–1016. https://doi.org/10.1029/1999GL002376.

Harrison, E.L., Veron, F., Ho, D.T., Reid, M.C., Orton, P., McGillis, W.R., 2012. Nonlinear interaction between rain- and wind-induced air-water gas exchange. J. Geophys. Res. Oceans 117 (C3), C03034. https://doi.org/10.1029/2011JC007693.

Hernández-Guerra, A., Fraile-Nuez, E., López-Laatzen, F., Martínez, A., Parrilla, G., Vélez-Belchí, P., 2005. Canary current and north equatorial current from an inverse box model. J. Geophys. Res. Oceans 110, C12019. https://doi.org/10.1029/2005JC003032.

van Heuven, S., Pierrot, D., Rae, J.W.B., Lewis, E., Wallace, D.W.R., 2011. MATLAB Program Developed for CO2 System Calculations. Carbon Dioxide Information Analysis Center, Oak Ridge National Laboratory, U.S. Department of Energy, Oak Ridge, Tennessee https://doi.org/10.3334/CDIAC/otg.CO2SYS_MATLAB_v1.1 Retrieved from.

Ho, D.T., Schanze, J.J., 2020. Precipitation-induced reduction in surface ocean pCO2: observations from the eastern tropical Pacific Ocean. Geophys. Res. Lett. 47 (15). https://doi.org/10.1029/2020GL088252 e2020GL088252.

Ho, D.T., Asher, W.E., Bliven, L.F., Schlosser, P., Gordan, E.L., 2000. On mechanisms of rain-induced air-water gas exchange. J. Geophys. Res. 105 (C10), 24045–24057. https://doi.org/10.1029/1999jc000280.

Ho, D.T., Law, C.S., Smith, M.J., Schlosser, P., Harvey, M., Hill, P., 2006. Measurements of air-sea gas exchange at high wind speeds in the Southern Ocean: implications for global parameterizations. Geophys. Res. Lett. 33 (15), L16611. https://doi.org/10.1029/2006GL026817.

Huffman, G.J., Adler, R.F., Bolvin, D.T., Gu, G., Nelkin, E.J., Bowman, K.P., et al., 2007. The TRMM Multisatellite Precipitation Analysis (TMPA): quasi-global, multiyear, combined-sensor precipitation estimates at fine scales. J. Hydrometeorol. 8, 38. https://doi.org/10.1175/JHM560.1.

Ibánhez, J.S.P., Diverrès, D., Araujo, M., Lefèvre, N., 2015. Seasonal and interannual variability of sea-air CO2 fluxes in the tropical Atlantic affected by the Amazon River plume. Glob. Biogeochem. Cycles 29 (10). https://doi.org/10.1002/2015GB005110 2015GB005110.

Ibánhez, J.S.P., Araujo, M., Lefèvre, N., 2016. The overlooked tropical oceanic CO2 sink. Geophys. Res. Lett. 43 (8), 3804–3812. https://doi.org/10.1002/2016GL068020.

Ibánhez, J.S.P., Flores, M., Lefèvre, N., 2017. Collapse of the tropical and subtropical North Atlantic CO2 sink in boreal spring of 2010. Sci. Rep. 7, 41694. https://doi.org/10.1038/srep41694.

Johnson, M.S., Meskhidze, N., 2013. Atmospheric dissolved iron deposition to the global oceans: effects of oxalate-promoted Fe dissolution, photochemical redox cycling, and dust mineralogy. Geosci. Model Dev. 6 (4), 1137–1155. https://doi.org/10.5194/gmd-6-1137-2013.

Kang, S.M., Shin, Y., Xie, S.-P., 2018. Extratropical forcing and tropical rainfall distribution: energetics framework and ocean Ekman advection. NPJ Clim. Atmos. Sci. 1 (1), 1–10. https://doi.org/10.1038/s41612-017-0004-6.

Körtzinger, A., 2003. A significant CO2 sink in the tropical Atlantic Ocean associated with the Amazon River plume. Geophys. Res. Lett. 30 (24), 2287. https://doi.org/10.1029/2003GL018841.

Körtzinger, A., 2010. The outer Amazon plume: an atmospheric CO2 sink. In: Liu, K.-K., Atkinson, L., Quiñones, R., Talaue-McManus, L. (Eds.), Carbon and Nutrient Fluxes in Continental Margins: A Global Synthesis. Springer, New York, USA, pp. 450–453.

Kustka, A., Carpenter, E.J., Sañudo-Wilhelmy, S.A., 2002. Iron and marine nitrogen fixation: progress and future directions. Res. Microbiol. 153 (5), 255–262. https://doi.org/10.1016/S0923-2508(02)01325-6.

Landschützer, P., Gruber, N., Bakker, D.C.E., 2016. Decadal variations and trends of the global ocean carbon sink. Glob. Biogeochem. Cycles 30 (10), 1396–1417. https://doi.org/10.1002/2015GB005359.

Lefèvre, N., 2009. Low CO2 concentrations in the Gulf of Guinea during the upwelling season in 2006. Mar. Chem. 113 (1–2), 93–101. https://doi.org/10.1016/j.marchem.2009.01.001.

Lefèvre, N., Diverrès, D., 2021a. Seawater Fugacity of CO2 in the Tropical Atlantic From 2008 to 2014. SEANOE https://doi.org/10.17882/84523.

Lefèvre, N., Diverrès, D., 2021b. Atmospheric Fugacity of CO2 in the Tropical Atlantic From 2008 to 2014. SEANOE https://doi.org/10.17882/84526.

Lefèvre, N., Diverrès, D., Gallois, F., 2010. Origin of CO2 undersaturation in the western tropical Atlantic. Tellus B 62 (5), 595–607. https://doi.org/10.1111/j.1600-0889.2010.00475.x.

Lefèvre, N., Caniaux, G., Janicot, S., Gueye, A.K., 2013. Increased CO2 outgassing in February-May 2010 in the tropical Atlantic following the 2009 Pacific El Niño. J. Geophys. Res. Oceans 118 (4), 1645–1657. https://doi.org/10.1002/jgrc.20107.

Lefèvre, N., Urbano, D.F., Gallois, F., Diverrès, D., 2014. Impact of physical processes on the seasonal distribution of the fugacity of CO2 in the western tropical Atlantic. J. Geophys. Res. Oceans 119 (2), 646–663. https://doi.org/10.1002/2013JC009248.

Lefèvre, N., Flores Montes, M., Gaspar, F.L., Rocha, C., Jiang, S., Araújo, D., et al., 2017a. Net heterotrophy in the Amazon continental shelf changes rapidly to a sink of CO2 in the outer Amazon plume. Front. Mar. Sci. 4, 278. https://doi.org/10.3389/fmars.2017.00278.

Lefèvre, N., da Silva Dias, F.J., de Torres Jr, A.R., Noriega, C., Araujo, M., de Castro, A.C.L., Rocha, C., Jiang, S., Ibánhez, J.S.P., 2017b. A source of CO2 to the atmosphere throughout the year in the Maranhense continental shelf (2°30′S, Brazil). Cont. Shelf Res. 141, 38–50. https://doi.org/10.1016/j.csr.2017.05.004.

Lefèvre, N., Veleda, D., Tyaquiçã, P., Perruche, C., Diverrès, D., Ibánhez, J.S.P., 2019. Basin-scale estimate of the sea-air CO2 flux during the 2010 warm event in the tropical North Atlantic. J. Geophys. Res. Biogeosci. 124 (4), 973–986. https://doi.org/10.1029/2018JG004840.

Lefèvre, N., Tyaquiçã, P., Veleda, D., Perruche, C., van Gennip, S.J., 2020. Amazon River propagation evidenced by a CO2 decrease at 8°N, 38°W in September 2013. J. Mar. Syst. 211, 103419. https://doi.org/10.1016/j.jmarsys.2020.103419.

Lübbecke, J.F., Rodríguez-Fonseca, B., Richter, I., Martín-Rey Marta, M., Losada, T., Polo, I., Keenlyside, N.S., 2018. Equatorial Atlantic variability—modes, mechanisms, and global teleconnections. Wiley Interdiscip. Rev. Clim. Chang. 9, e527. https://doi.org/10.1002/wcc.527.

Mahowald, N.M., Engelstaedter, S., Luo, C., Sealy, A., Artaxo, P., Benitez-Nelson, C., et al., 2009. Atmospheric iron deposition: global distribution, variability, and human perturbations. Annu. Rev. Mar. Sci. 1 (1), 245–278. https://doi.org/10.1146/annurev.marine.010908.163727.

Mehrbach, C., Culberson, C.H., Hawley, J.E., Pytkowicx, R.M., 1973. Measurement of the apparent dissociation constants of carbonic acid in seawater at atmospheric pressure1. Limnol. Oceanogr. 18 (6), 897–907. https://doi.org/10.4319/lo.1973.18.6.0897.

Meskhidze, N., Chameides, W.L., Nenes, A., 2005. Dust and pollution: a recipe for enhanced ocean fertilization? J. Geophys. Res. Atmos. 110, D03301. https://doi.org/10.1029/2004JD005082.

Mignot, J., Lazar, A., Lacarra, M., 2012. On the formation of barrier layers and associated vertical temperature inversions: A focus on the northwestern tropical Atlantic. J. Geophys. Res. 117, C02010. https://doi.org/10.1029/2011JC007435.

Moore, C. Mark, Mills, M.M., Achterberg, E.P., Geider, R.J., LaRoche, J., Lucas, M.I., et al., 2009. Large-scale distribution of Atlantic nitrogen fixation controlled by iron availability. Nat. Geosci. 2 (12), 867–871. https://doi.org/10.1038/ngeo667.

Moore, C.M., Mills, M.M., Arrigo, K.R., Berman-Frank, I., Bopp, L., Boyd, P.W., et al., 2013. Processes and patterns of oceanic nutrient limitation. Nat. Geosci. 6 (9), 701–710. https://doi.org/10.1038/ngeo1765.

Mulholland, M.R., Capone, D.G., 2001. Stoichiometry of nitrogen and carbon utilization in cultured populations of Trichodesmium IMS101: implications for growth. Limnol. Oceanogr. 46 (2), 436–443. https://doi.org/10.4319/lo.2001.46.2.0436.

O'Reilly, J.E., Maritorena, S., Mitchell, B.G., Siegel, D.A., Carder, K.L., Garver, S.A., et al., 1998. Ocean color chlorophyll algorithms for SeaWiFS. J. Geophys. Res. Oceans 103 (C11), 24937–24953. https://doi.org/10.1029/98JC02160.

Oudot, C., Ternon, J.F., Lecomte, J., 1995. Measurements of atmospheric and oceanic CO2 in the tropical Atlantic: 10 years after the 1982-1984 FOCAL cruises. Tellus Ser. B Chem. Phys. Meteorol. 47 (1–2), 70–85. https://doi.org/10.3402/tellusb.v47i1-2.16032.

Pickett, M.H., Paduan, J.D., 2003. Ekman transport and pumping in the California Current based on the US Navy's high-resolution atmospheric model (COAMPS). J. Geophys. Res. Oceans 108 (C10), 1–10. https://doi.org/10.1029/2003JC001902.

Pierrot, D., Neill, C., Sullivan, K., Castle, R., Wanninkhof, R., Lüger, H., et al., 2009. Recommendations for autonomous underway pCO2 measuring systems and data-reduction routines. Deep-Sea Res. II Top. Stud. Oceanogr. 56 (8–10), 512–522. https://doi.org/10.1016/j.dsr2.2008.12.005.

Prospero, J.M., Collard, F.-X., Molinié, J., Jeannot, A., 2014. Characterizing the annual cycle of African dust transport to the Caribbean Basin and South America and its impact on the environment and air quality. Glob. Biogeochem. Cycles 28 (7), 757–773. https://doi.org/10.1002/2013GB004802.

Richter, I., Tokinaga, H., 2021. The Atlantic Niño: dynamics, thermodynamics, and teleconnections. In: Behera, S.K. (Ed.), Tropical and Extra-tropical Air-sea Interactions. Elsevier, pp. 171–206.

Sarmiento, J.L., Gruber, N., 2006. Ocean Biogeochemical Dynamics. Princeton University Press.

Schlosser, C., Klar, J.K., Wake, B.D., Snow, J.T., Honey, D.J., Woodward, E.M.S., et al., 2014. Seasonal ITCZ migration dynamically controls the location of the (sub)tropical Atlantic biogeochemical divide. Proc. Natl. Acad. Sci. 111 (4), 1438–1442. https://doi.org/10.1073/pnas.1318670111.

Servain, J., Caniaux, G., Kouadio, Y.K., McPhaden, M.J., Araujo, M., 2014. Recent climatic trends in the tropical Atlantic. Clim. Dyn. 43 (11), 3071–3089. https://doi.org/10.1007/s00382-014-2168-7.

Stramma, L., 1991. Geostrophic transport of the South Equatorial Current in the Atlantic. J. Mar. Res. 49, 281–294. https://doi.org/10.1357/002224091784995864.

Subramaniam, A., Yager, P.L., Carpenter, E.J., Mahaffey, C., Björkman, K., Cooley, S., et al., 2008. Amazon River enhances diazotrophy and carbon sequestration in the tropical North Atlantic Ocean. Proc. Natl. Acad. Sci. 105 (30), 10460–10465. https://doi.org/10.1073/pnas.0710279105.

Subramaniam, Ajit, Mahaffey, C., Johns, W., Mahowald, N., 2013. Equatorial upwelling enhances nitrogen fixation in the Atlantic Ocean. Geophys. Res. Lett. 40 (9), 1766–1771. https://doi.org/10.1002/grl.50250.

Takahashi, T., Sutherland, S.C., Wanninkhof, R., Sweeney, C., Feely, R.A., Chipman, D.W., et al., 2009. Climatological mean and decadal change in surface ocean pCO2, and net sea–air CO2 flux over the global oceans. Deep-Sea Res. II Top. Stud. Oceanogr. 56 (8–10), 554–577. https://doi.org/10.1016/j.dsr2.2008.12.009.

Takahashi, T., Sutherland, S.C., Chipman, D.W., Goddard, J.G., Ho, C., Newberger, T., et al., 2014. Climatological distributions of pH, pCO2, total CO2, alkalinity, and CaCO3 saturation in the global surface ocean, and temporal changes at selected locations. Mar. Chem. 164, 95–125. https://doi.org/10.1016/j.marchem.2014.06.004.

Ternon, J.F., Oudot, C., Dessier, A., Diverres, D., 2000. A seasonal tropical sink for atmospheric CO2 in the Atlantic ocean: the role of the Amazon River discharge. Mar. Chem. 68 (3), 183–201. https://doi.org/10.1016/S0304-4203(99)00077-8.

Turk, D., Zappa, C.J., Meinen, C.S., Christian, J.R., Ho, D.T., Dickson, A.G., McGillis, W.R., 2010. Rain impacts on CO2 exchange in the western equatorial Pacific Ocean. Geophys. Res. Lett. 37 (23), L23610. https://doi.org/10.1029/2010GL045520.

Tyaquiçã, P., Veleda, D., Lefèvre, N., Araujo, M., Noriega, C., Caniaux, G., Servain, J., Silva, T., 2017. Amazon plume salinity response to ocean teleconnections. Front. Mar. Sci. 4, 250. https://doi.org/10.3389/fmars.2017.00250.

Weiss, R.F., 1974. Carbon dioxide in water and seawater: the solubility of a non-ideal gas. Mar. Chem. 2 (3), 203–215. https://doi.org/10.1016/0304-4203(74)90015-2.

Woolf, D.K., Shutler, J.D., Goddijn-Murphy, L., Watson, A.J., Chapron, B., Nightingale, P.D., et al., 2019. Key uncertainties in the recent air-sea flux of CO2. Glob. Biogeochem. Cycles 33 (12), 1548–1563. https://doi.org/10.1029/2018GB006041.

Zamora, L.M., Prospero, J.M., Hansell, D.A., Trapp, J.M., 2013. Atmospheric P deposition to the subtropical North Atlantic: sources, properties, and relationship to N deposition. J. Geophys. Res. Atmos. 118 (3), 1546–1562. https://doi.org/10.1002/jgrd.50187.

Zhang, D., McPhaden, M.J., Johns, W.E., 2003. Observational evidence for flow between the subtropical and tropical Atlantic: the Atlantic subtropical cells. J. Phys. Oceanogr. 33 (8), 1783–1797. https://doi.org/10.1175/2408.1.